Photocopy and Use Authorization

In presenting this thesis in partial fulfillment of the requirements for an advanced degree at Idaho State University, I agree that the Library shall make it freely available for inspection. I further state that permission for extensive copying of my thesis for scholarly purposes may be granted by the Dean of the Graduate School, Dean of my academic division, or by the University Librarian. It is understood that any copying or publication of this thesis for financial gain shall not be allowed without my written permission.

Signature _____

Date _____

Creating a Monte Carlo N-Particle (MCNP) Simulation of an Uncontrolled Source to Estimate Dose Rates in Office Spaces Outside the Laboratory Area

By

Mikayla J. Thompson

A thesis

submitted in partial fulfillment

of the requirements for the degree of

Master of Science in the Department of Nuclear Engineering and Health Physics

Idaho State University

April 2023

To the Graduate Faculty:

The members of the committee appointed to examine the thesis of Mikayla J. Thompson find it satisfactory and recommend that it be accepted.

_____

Dr. Chad L. Pope,
Major Advisor

_____

Dr. Richard R. Brey,
Committee Member

_____

Dr. Daniel LaBrier,
Committee Member

_____

Dr. Bruce Savage
Graduate Faculty Representative

Acknowledgements

This research made use of the resources of the High Performance Computing Center at Idaho National Laboratory, which is supported by the Office of Nuclear Energy of the U.S. Department of Energy and the Nuclear Science User Facilities under Contract No. DE-AC07-05ID14517.

I want to thank Idaho National Laboratory for providing the work environment for this project to take place. Leonard Davis, the HPIL Manager who provided the MCNP license for me to perform my work. Thayne Butikofer and Emily Smith, Radiological Engineers at HPIL, who assisted with my source viewing experiment. Dr. Edward Seabury, who placed my simulations on the HPC. Dr. Matt Meengs, who graciously taught me how to use MCNP and checked my input deck multiple times for errors. Wade Scates, for helping me with MCNP and volunteering to be a reviewer for my INL documentation of this project.

Finally, I'd like to thank my family, especially my husband, Dr. Zachary Thompson, for spending several weekends helping me problem solve, teaching me how to use the plot window in MCNP, and for practically being a single parent for two years while I completed this program. To my kids for being patient with mommy while she finished her masters. I hope my efforts will be an example to them to never give up on your dreams, no matter how hard or inconvenient they may be. I promise mommy is done working weekends.

Table of Contents

List of Figures

List of Tables

Creating a Monte Carlo N-Particle (MCNP) Simulation of an Uncontrolled Source to Estimate Dose Rates in Office Spaces Outside the Laboratory Area

Thesis Abstract – Idaho State University (April 2023)

An MCNP simulation was created for the Health Physics Instrument Laboratory (HPIL) at the Idaho National Laboratory (INL) to determine potential safe evacuation zones in the event of an uncontrolled, high activity ^{137}Cs source during non-routine operations. An experimental comparison test case was developed to demonstrate the performance of the MCNP simulation. The experiment consisted of placing meters in the laboratory and offices during a source viewing. The experimental data was compared to the MCNP simulated results. The simulation was determined to produce usable results when meter readings and simulated detector readings fell within 21% of each other. Outlier positional data could be due to slight variations in building geometry or sources of scatter not considered in the simulations. Seven source positions were simulated, and two general evacuation zones were determined from these simulations: the lobby/front offices and loading dock areas.

Keywords: shielding, uncontrolled source, dose simulation, MCNP

1 INTRODUCTION

At the Health Physics Instrument Laboratory (HPIL) at Idaho National Laboratory (INL), there are six irradiator systems with individual or multiple radioactive sources held within. These systems are used for the calibration of health physics instruments and include both gamma and neutron sources. The sources, or "rabbits," are actuated to their exposure positions through either high-pressure air systems or by a platform raising and lower the source. There are occasions when these systems need to be serviced in a manner requiring the sources be removed from the system and stored or exposed above the shielded exposure apparatus. In each of these use cases, there are inherent risks the source may become uncontrolled. Discussions with Radiological Control about what to do in the event of an uncontrolled source vary from evacuating to the front half of the HPIL building to evacuating to the parking lot. This thesis serves to establish potential safe evacuation zones if the largest of the ^{137}Cs sources (1250 Ci) becomes uncontrolled at any point in operations using Monte Carlo N-Particle (MCNP) simulations.

2 BACKGROUND

2.1 Cs-137: Decay mechanisms, properties, interaction potential

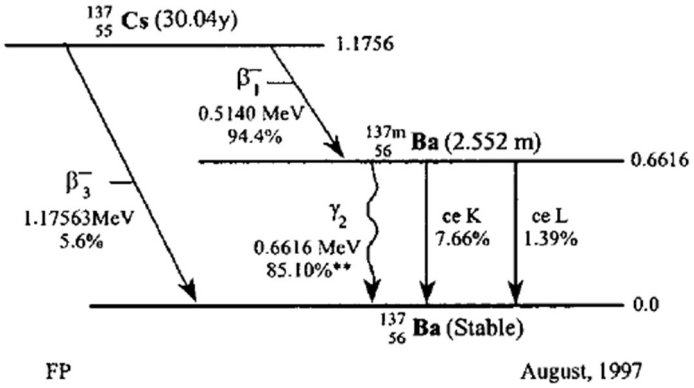

Radiation	Y_i (%)	E_i (MeV)
β^-_1	94.40	0.1734*
β^-_3	5.60	0.4163*
γ_2	85.10**	0.6617
ce-K, γ_1	7.66	0.6242
ce-L, γ_1	1.39	0.6557
Kα1 X-ray	3.61	0.0322
Kα2 X-ray	1.96	0.0318
Kβ X-ray	1.33	0.0364*
L X-ray	0.91	0.0045*
Auger-K	0.76	0.0264*
Auger-L	7.20	0.0367*

* Average Energy

Figure 1: ^{137}Cs decay schematic [25]

^{137}Cs is decays via β^- to ^{137m}Ba with 94.4% yield or to ^{137}Ba with 5.6% yield (see Figure 1). The 0.662 MeV gamma typically associated with a ^{137}Cs source is a product of the ^{137m}Ba settling to a stable state with a yield of 85.1%. ^{137}Cs has a half-life of 30.1671 years and is in secular equilibrium with ^{137m}Ba [17]. Secular equilibrium occurs when the half-life of the progeny is much shorter than the parent [25]. This allows for the progeny activity to build-up to nearly the same amount as the parent.

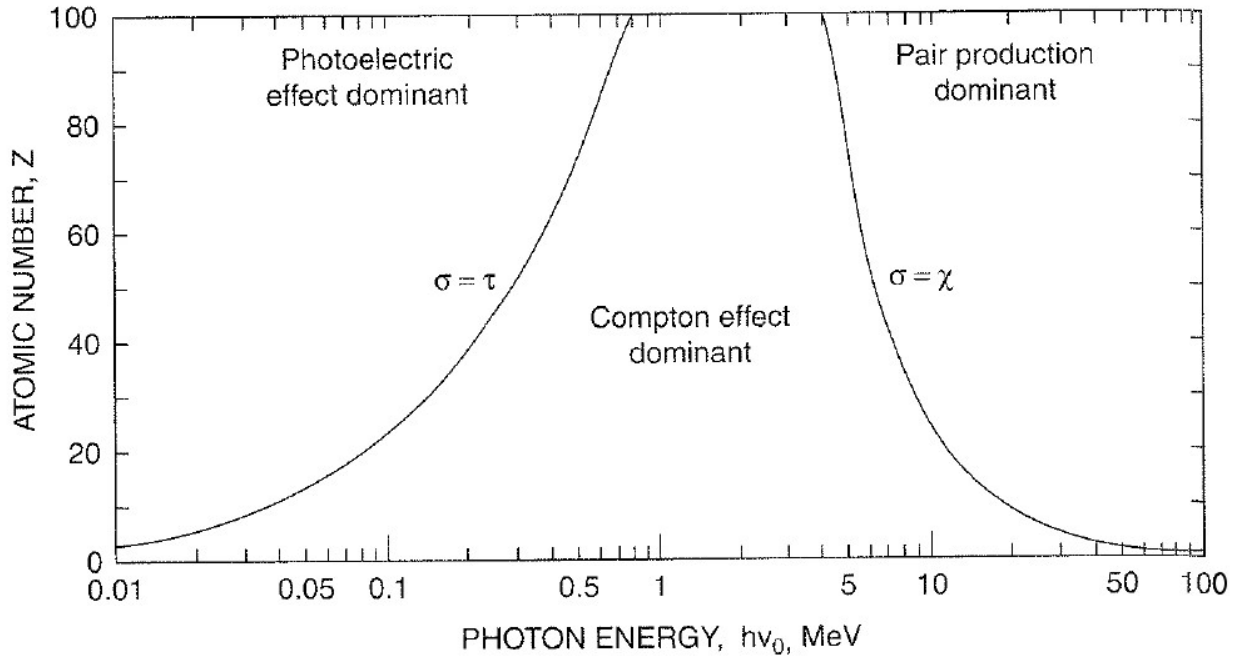

Figure 2: Dominant interaction for photons of energy MeV and atomic number of the material [21]

Figure 2 shows the interaction probability as a function of photon energy and atomic number of the interaction materials, from which the determination of the primary interactions for ^{137}Cs can be determined. The 0.662 MeV photon produced during the decay of ^{137}Cs typically interacts with matter through either the photoelectric effect or Compton scattering. The photoelectric effect occurs when a photon interacts with an electron, causing all energy to be transferred to the electron, and the electron is ejected from the atom [4]. The energy from the photon is used to overcome the binding energy of the electron and the rest is transferred directly to the electron in the form of kinetic energy [2]. The result is a characteristic x-ray when another electron fills the vacancy left by the ejected electron. The photoelectric effect is the desirable interaction for shielding materials as it absorbs the entire photon [4]. The photoelectric effect is most probable with low energy photons (less than the rest mass energy of an electron 0.511 MeV) and with high atomic number/density materials [4].

Compton scattering is a form of incoherent scattering, meaning the photon loses some energy and changes direction (scatters) as a result of the interaction [4]. This interaction occurs when a photon interacts with a loosely bound outer shell election, transferring some of its energy to the electron, forcing the electron out of the atom in a direction, and the photon scatters in a different direction [4]. The resulting energy of the scattered particles can be calculated using the angle of scatter for the photon. Equation 1 is used to determine the energy of the electron and scattered photon [4].

$$E_{\gamma}^{'} = \frac{E_{\gamma}}{1 + \left(\frac{E_{\gamma}}{511\ keV}\right)(1 - cos\theta)}$$

$$E_e = E_{\gamma} - E_{\gamma}^{'}$$

where

$$E_{\gamma} = initial\ photon\ energy$$

$$E_{\gamma}^{'} = scattered\ photon\ energy$$

$$\theta = photon\ scatter\ angle$$

$$E_e = kinetic\ energy\ of\ scattered\ electron$$

Equation 1

Pair production is not possible for ^{137}Cs because the photon energy is too low. No interaction produced by a ^{137}Cs photon interaction can produce a higher energy particle than the 0.662 MeV initial photon, as would be required for pair production.

^{137}Cs is commonly used as a source for calibration laboratories because it is a fission product and the associated gamma is lower energy than those found around nuclear materials [2]. This makes it a conservative source for calibrations. For the INL, this source was chosen based on the typical source terms experienced in facilities.

2.2 Hopewell Designs, Inc. (HDI) – Gamma Beam Irradiator (GBI)

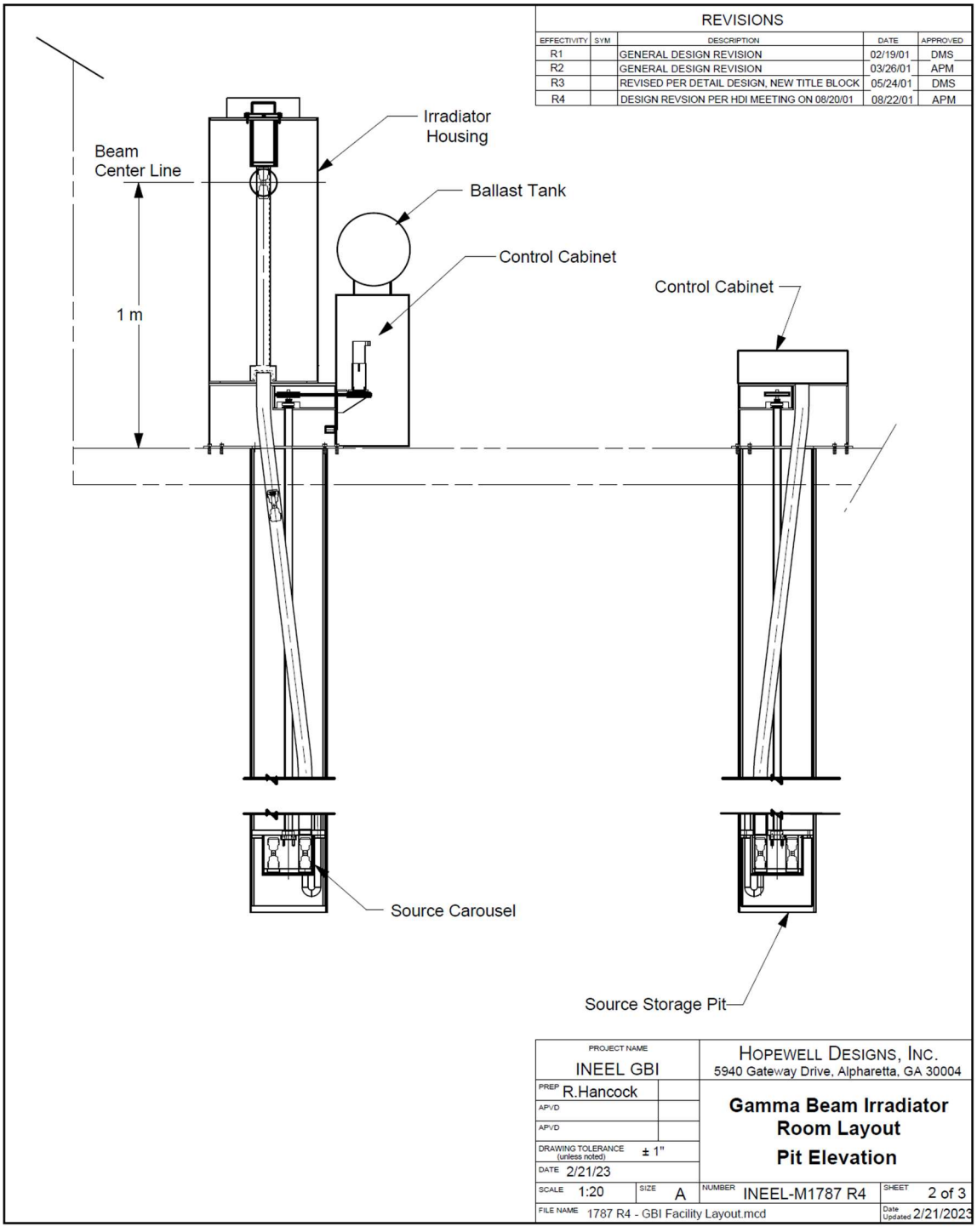

Figure 3: Gamma Beam Irradiator Room Layout Pit Elevation (Hopewell Designs, INC.) [12]

Hopewell Designs, Inc. (HDI) designed and installed the Gamma Beam Irradiator (GBI) in 2002. This irradiator contains 8 individual source rabbits: 3 Ci ^{60}Co, 281 Ci ^{60}Co, 20 mCi ^{137}Cs, 500 mCi ^{137}Cs, 10 Ci ^{137}Cs, 100 Ci ^{137}Cs, 1250 Ci ^{137}Cs, and a dummy (all activities listed are at the time of installation) [8, 9]. The sources are stored in a carousel eight feet below the laboratory floor, rotating to expose the desired source rabbit as selected in the control panel [22].

Figure 3 shows the below grade source carousel and the rabbit's path to exposure in the collimator [12]. Once the carousel has rotated to the correct source position, the control key is turned to the ENABLE position and the EXPOSE button is pressed to tell the system to move the source rabbit to the exposed position [22]. Solenoids actuate the air flow to move the source rabbit out of its carousel position into the exposed position. After the air function has been initiated, the source rabbit impacts a suction cup, which triggers a sensor to begin applying a vacuum through the suction cup. This vacuum is applied until the RETURN button is pressed, the desired dose has been achieved, or an error occurs inducing a fail-safe to return the source to storage.

The source rabbit sits in an exposed position within a lead collimator [15]. The aperture has optional attenuator panels allowing the user to reduce the beam strength by a factor of 2 to 8,000 [22]. The control panel within the computer system allows the user to select the source rabbit; the dose rate or dose; the attenuator positions during an exposure; and controls the x, z, and rotational axis of the instrument cart. The instrument cart has a maximum travel of 468.3 cm in the x direction, 29.4 cm in the z direction and can rotate 180 degrees. The flexibility in the instrument cart positions allows for a wide range of exposure rates to be experienced by instruments during calibration.

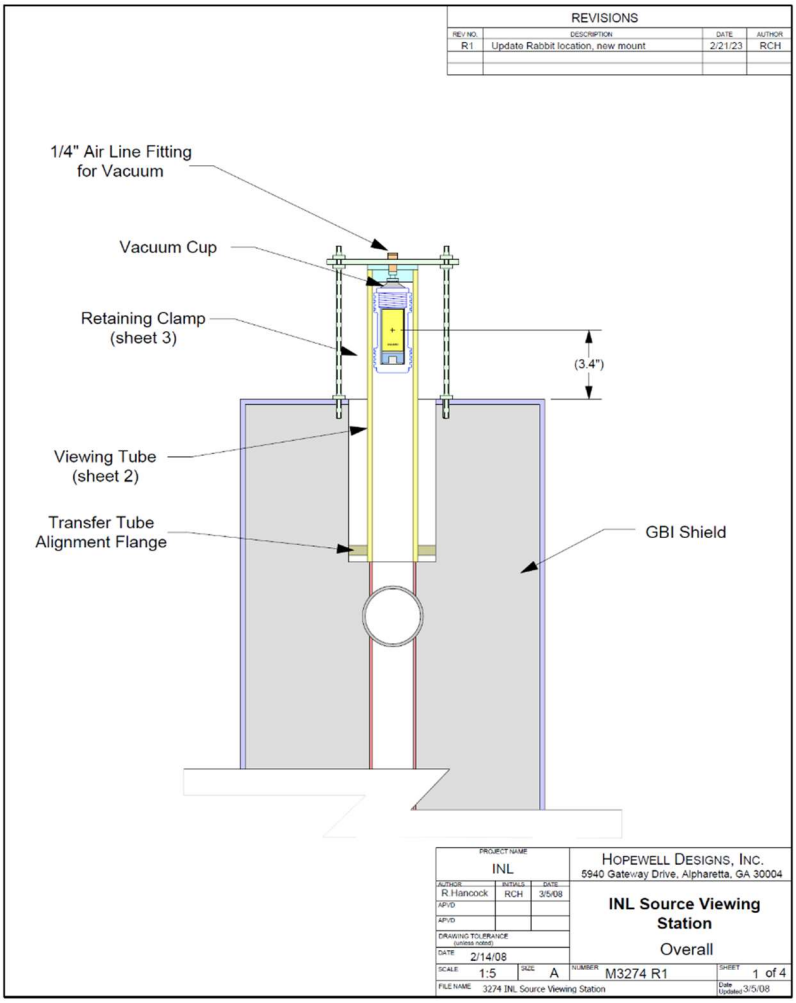

Figure 4: Source Viewing Port, GBI (Hopewell Designs, INC) [14]

HDI designed a source viewing port to view sources to ensure source rabbit integrity. This view port allows the source rabbit to travel beyond the height of the collimator into a clear, acrylic tube. Figure 4 is a schematic drawing showing how the source is able to travel above the shielding cylinder into the view port. The view port consists of an alignment flange, acrylic tube, retainment clamps, and opening to install the vacuum suction cup assembly [14].

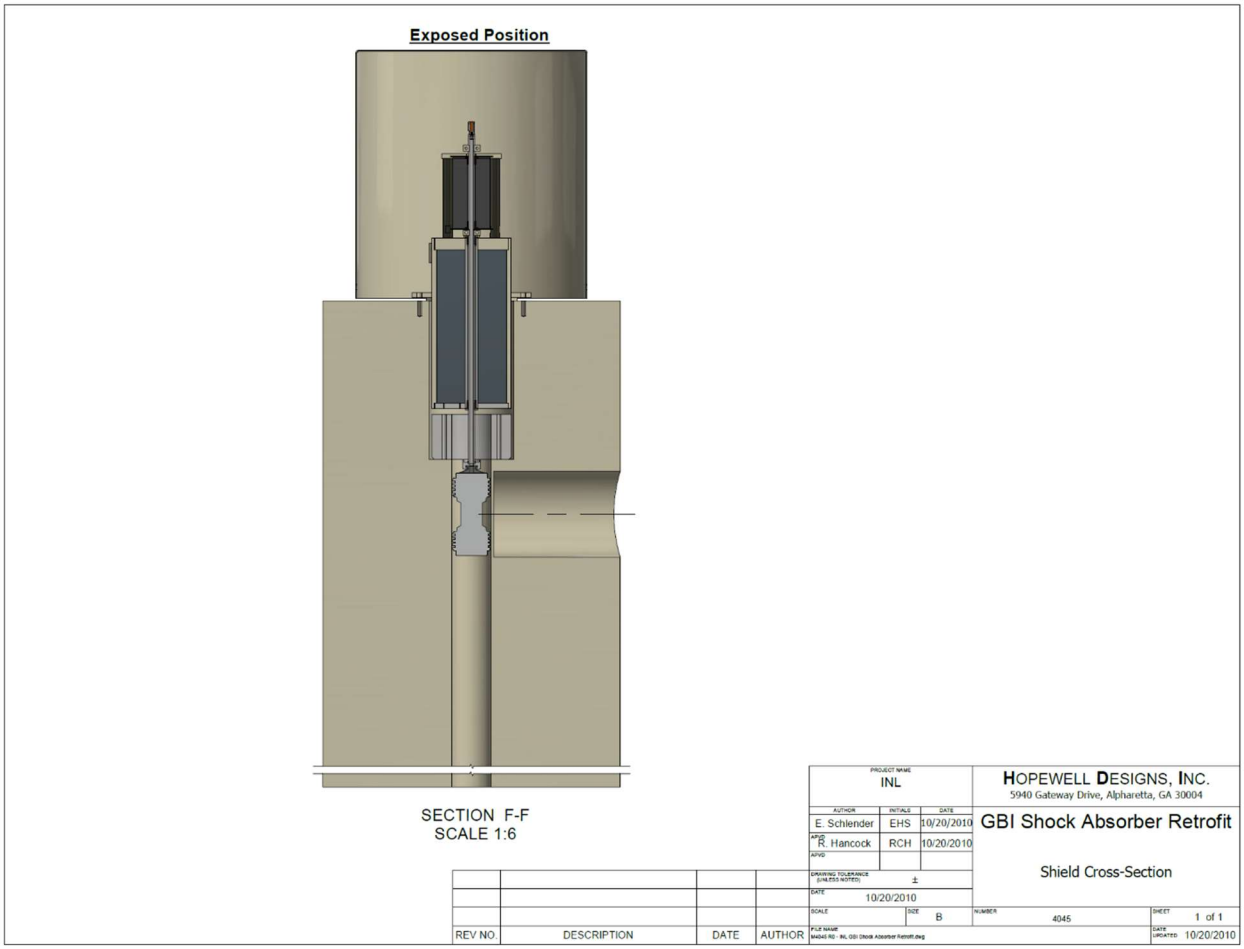

Figure 5: GBI Shock Absorber Retrofit (Hopewell Designs, INC) [15]

To install the view port, the exposure head, the assembly shown above the rabbit in Figure 5, is removed from the top of the collimator and the view port installed. Using an extended control panel within the Automated Irradiator System (AIS) software, the user can actuate the different air functions to rotate the source rabbit to view the entire source.

2.3 Source Rabbit Design

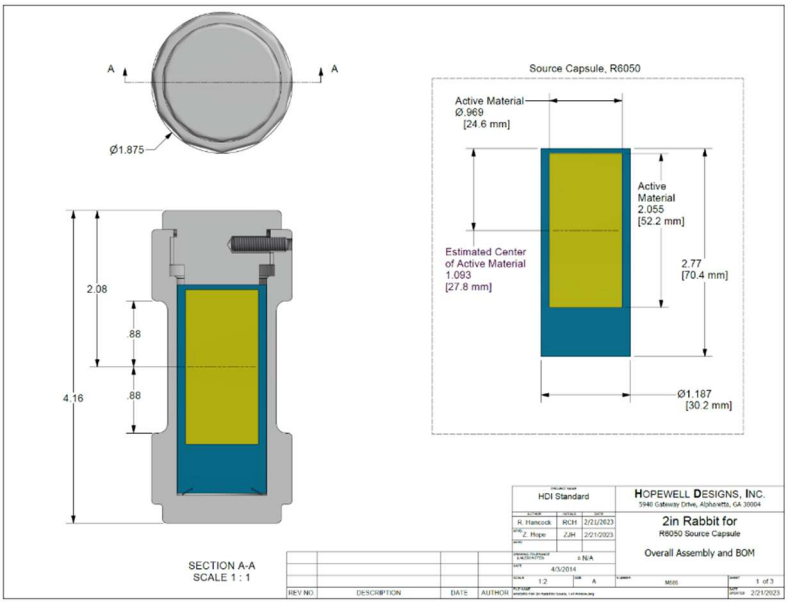

Figure 6: 2in Rabbit for R6050 Source Capsule pg 1 (Hopewell Designs, INC) [16]

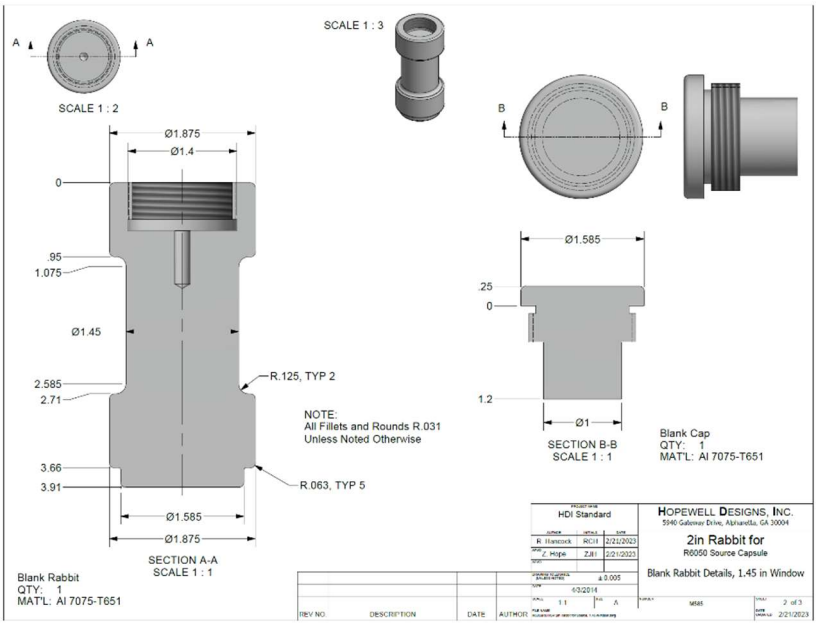

Figure 7: 2in Rabbit for R6050 Source Capsule pg 2 (Hopewell Designs, INC) [16]

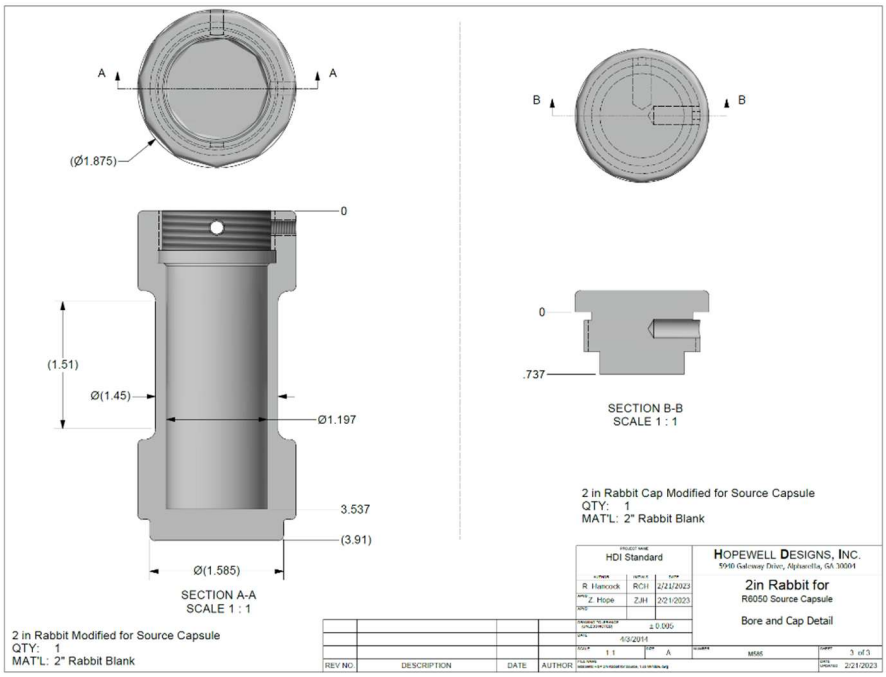

Figure 8: 2in Rabbit for R6050 source capsule pg 3 (Hopewell Designs, INC) [16]

The source rabbit for the 1250 Ci ^{137}Cs contains a capsule of cesium chloride measuring 70.4 mm x 30.2 mm, as shown in Figure 6 [16]. The capsule was placed in a spacer capsule to ensure the center of the source is at the center of the aluminum rabbit [16]. As shown in Figure 6, the capsule is inserted into an aluminum rabbit and sealed in with a screwed-on cap and set screw [16]. The final dimensions of the source rabbit are 4.16 in x 1.875 in [16]. From Figure 7 and Figure 8, the rabbit is narrower in the middle and expands on both ends [16]. This shape fills the travel tube, ensuring the rabbit is exposed in the same position every time.

2.4 Monte Carlo N-Particle (MCNP)

MCNP is a radiation transport code for "general-purpose, continuous-energy, generalized-geometry, time-dependent" simulations using 37 particle types over broad energy ranges [20]. The code has many uses from simulating reactor cores to shielding evaluations to detector pulse responses and many others. MCNP contains and applies a wide range of nuclear data to a user created input deck to simulate nuclear interactions with varying output options [10]. The user must

properly define the geometry, source term, materials, physics to be considered and simulated, multipliers and conversions to be applied, and define the desired output of the simulation [20].

For the purposes of this thesis, MCNP is being used to simulate dose rates in a facility when a ^{137}Cs source is placed, free in air, in various locations around the facility. For the desired output of dose rate, a multiplier and conversion factor must be applied to the MCNP output. The multiplier indicates the source strength while the conversion factor converts the output from particle fluence rate to dose rate [20]. This process will be explained in detail in the following section. MCNP version 6 was used for all simulations. The associated cross-section library for MCNP 6 is xdata/mcnplib84.

3 METHODOLOGY

3.1 Assumptions

Several assumptions were made to create the MCNP simulation. These assumptions simplified the geometry inputs, physics simulations, and source type. The first assumptions simplify the geometry of the building. For the MCNP simulations, the ceiling throughout the building is 6 inches (15.24 cm) of concrete at a height of 17 ft 4 in (529 cm) and the floor is a constant 6 in (15.24 cm) of concrete [19]. The actual ceiling height in the building varies from 10 ft to 19 ft with both hollow concrete and solid concrete ceilings varying from 6 in to 9 in thick [19]. For the purposes of simplification, the solid concrete portion of the ceiling is the only portion considered in this simulation. The potential effect of this simplification is variations in the potential photon scattering. In some areas, this simplification could decrease the simulated scatter and others it would increase the simulated scatter. The floors in the building are either sealed concrete, covered in tile, or covered with carpet. The assumption the floors are simply solid concrete should

not significantly change the results, as the tile and carpet surfaces will add little to the scattering effect on the simulated photons.

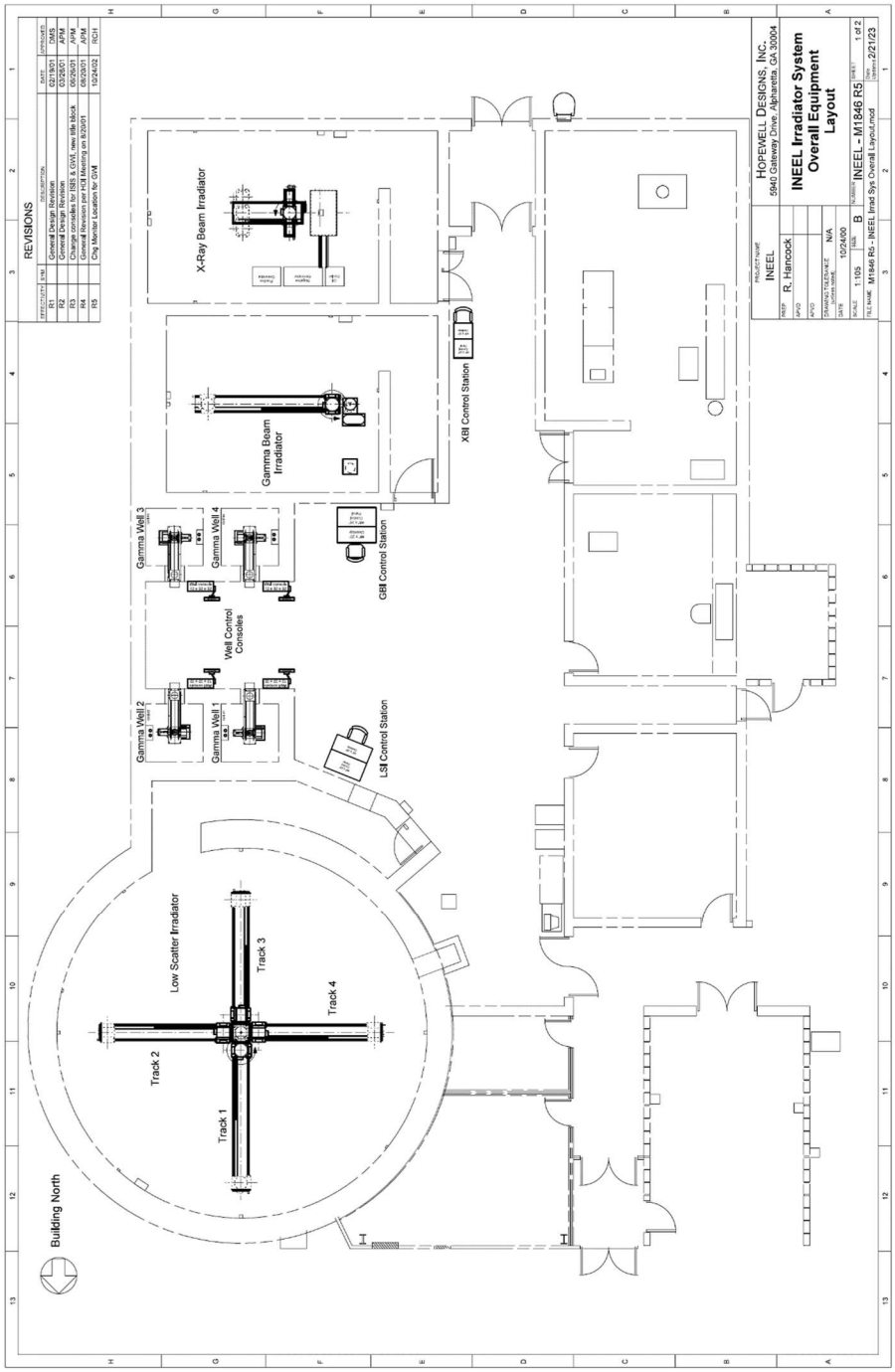

Figure 9: INEEL Irradiator System Overall Equipment Layout (Hopewell Designs, INC) [13]

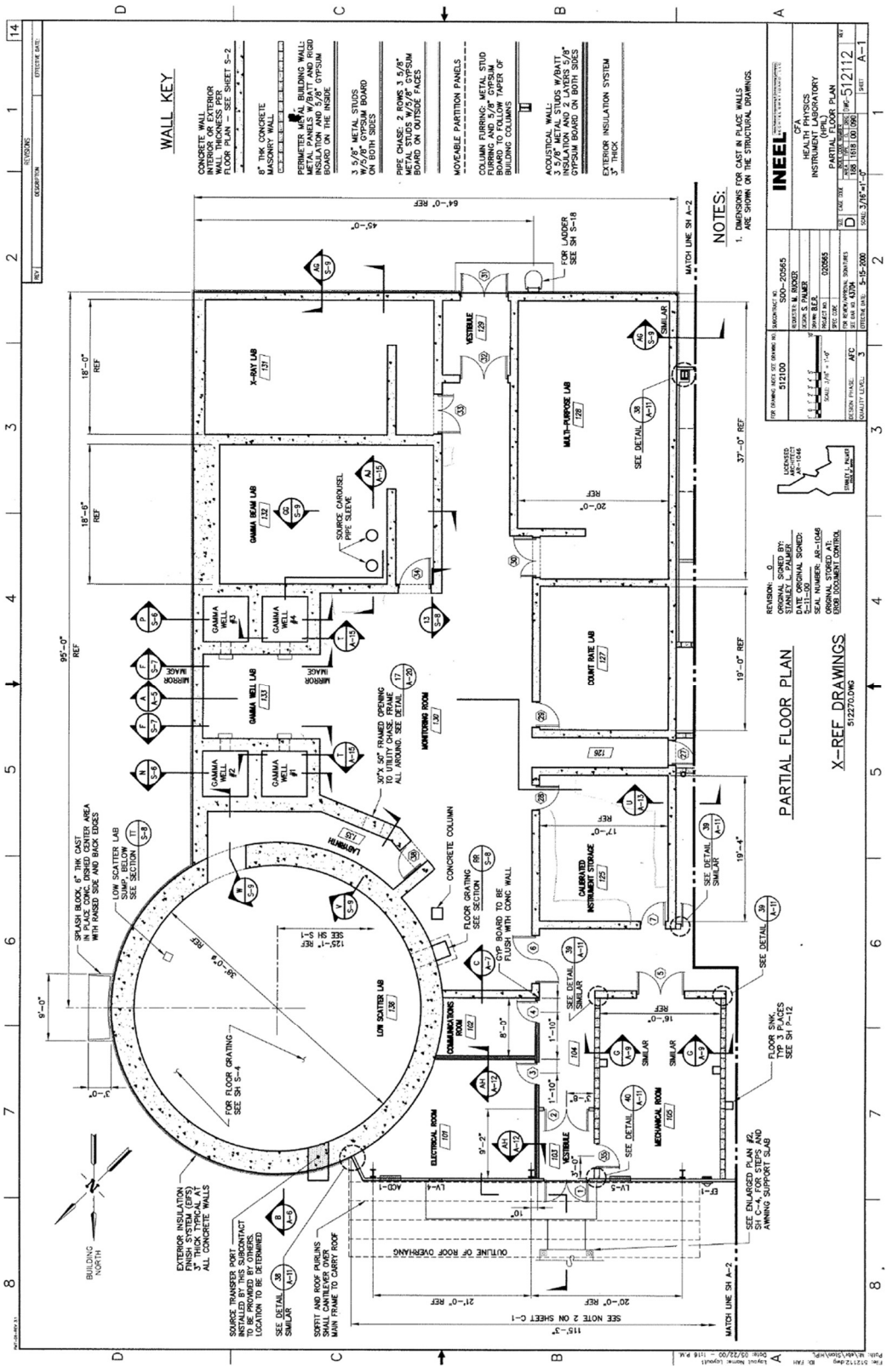

Figure 10: INEEL CFA Health Physics Instrument Laboratory (HPIL) Partial Floor Plan pg 14 [19]

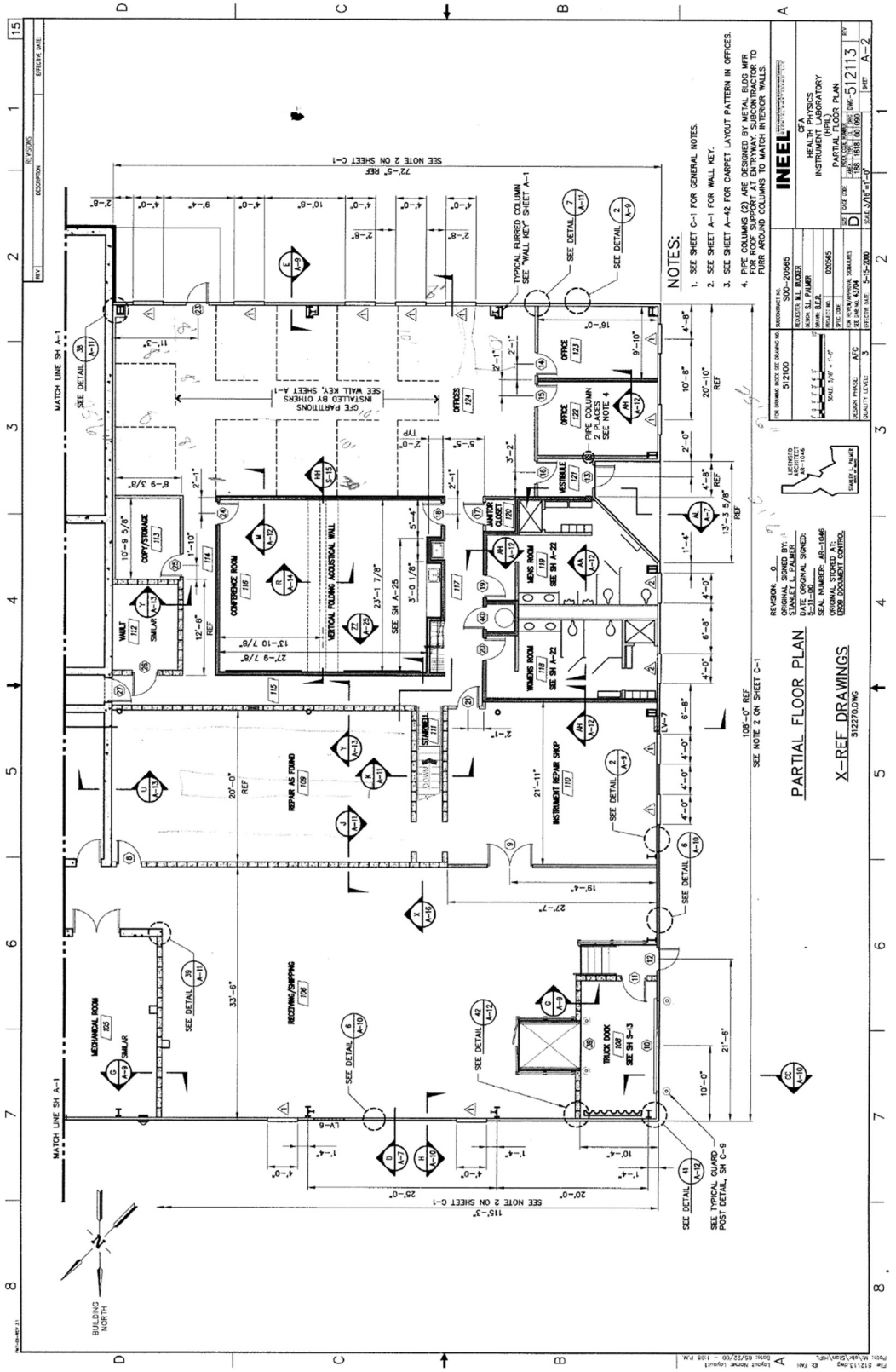

Figure 11: INEEL CFA Health Physics Instrument Laboratory (HPIL) Partial Floor Plan pg 15 [19]

The Low Scatter Irradiator (LSI), the cylindrical room in Figure 9, has a floor 13 feet below grade. The below grade area of the LSI has been ignored as it is not an area of interest for final simulations. The Gamma Well Irradiators (GWIs), labeled on Figure 9, also have openings in the concrete, laboratory facing walls, not included in the final simulation. The openings would reduce some scatter within the laboratory area, but not appreciably, and the interior of the GWIs is not an area of interest for the final simulations.

The second assumption is only concrete walls and forward exterior walls will be simulated. Figure 10 and Figure 11 show various other walls in the forward area of the building. The concrete shielding walls in and around the laboratory area are the largest source of attenuation and scatter. Some walls are cinder block construction, but the fill material is not specified in the drawings [19]. Omitting these walls will result in higher dose rates across wider areas of the building than would actually be seen. However, this will result in a conservative estimate of the resulting dose rates. It is known and understood there will be increased scatter down the corridor shown in Figure 11 between the “Vault” and “Repair As Found” areas and should be avoided during an event [19]. The areas of concern for this simulation are the “Offices”, “Truck Dock”, and “Instrument Repair Shop” (as labeled in Figure 11) [19]. These areas are the proposed evacuation assembly areas in the event of an uncontrolled source. The walls around the majority of the office space are standard cubicle walls and will not appreciably contribute to attenuation. The reduction in the radiation field will be affected more by the distance from the source.

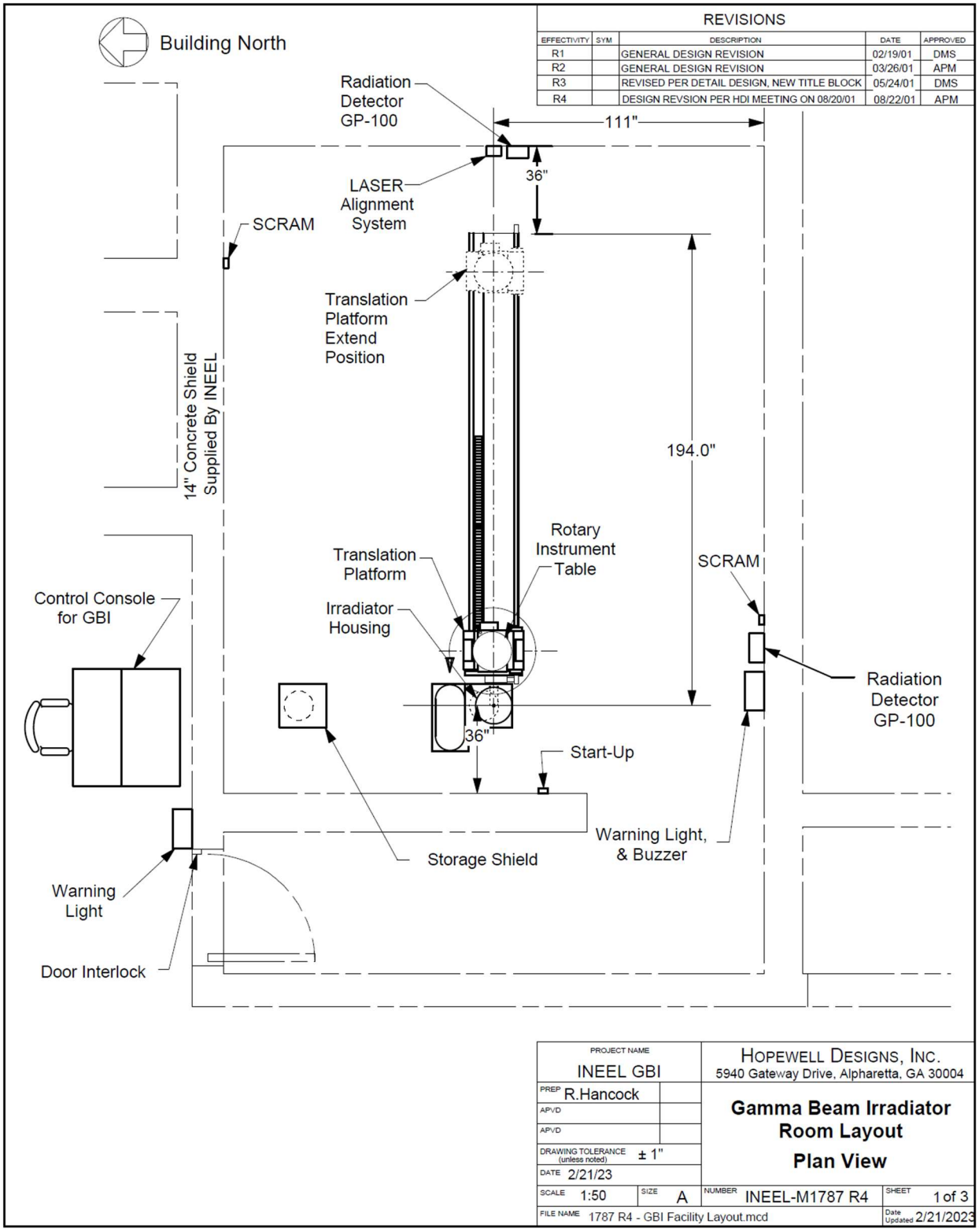

Figure 12: Gamma Beam Irradiator Room Layout Plan View [12]

The third assumption is the lead collimator, ballast tank, instrument cart, and control cabinet in the Gamma Beam Lab (GBL) will not be included in the model. Figure 12 shows these items, and others, present in the GBL. The only simulation this exclusion will affect is the experimental comparison test case simulation at Detector Position 1. For all other simulations, the source will be physically separated from the collimator and will not contribute to the dose rates in the areas of interest. This assumption will be addressed again in the results Experimental Comparison Test Case Results section.

The fourth assumption is all doors are air. This assumption was made because the doors in the lab areas provide little to no significant shielding. Some doors have glass windows in more than half of the surface area and the others are simply wood filled, stainless steel cased doors. In the event of an emergency, it is not guaranteed the doors would all be closed behind the evacuating staff members. For this reason, they are all input as air spaces in the MCNP simulation.

Assumption five is the source can be modeled as a point source. To apply point source geometry to a given problem, the areas of interest must 10 times the distance of the largest dimension of the source [4]. As Figure 6 shows, the largest dimension of the active area of the source capsule is 52.2 mm [16]. All areas of interest are significantly further from the source and therefore conform to the point source geometry assumption.

$$A = A_0 e^{-\lambda t}$$

where

$$A_0 = original\ activity = 1250\ Ci$$

$$\lambda = \frac{ln2}{t_{\frac{1}{2}}}$$

$$t_{\frac{1}{2}} = Half\ Life = 30.1671\ yr$$

$$t = time = 20.202600096\ yr$$

$$A = decayed\ activity$$

$$A = (1250\ Ci)e^{-\left(\frac{ln2}{30.1671\ yr}\right)(20.202600096\ yr)}$$

$$A = 785.8\ Ci$$

Equation 2

The final assumption is the activity of the source is decayed to October 19, 2022. The ^{137}Cs source being simulated was installed with 1250 Ci original activity. The decayed value of the source is 785.8 Ci. The Equation 2 shows how this value was produced [3]. The decay date chosen was the day the experiment comparison test was performed and therefore reflects the activity at the time of measurement.

3.2 MCNP Geometry and Materials Inputs

The HPIL building was built in 2002 as a state-of-the-art calibration facility. Several shielding evaluations were conducted using MCNP and other calculation methods to determine the necessary wall thicknesses for the given irradiator systems and proposed sources. These input decks have been lost to employee turnover and were not available for review. From these shielding evaluations, building drawings and schematics were produced. Using the construction drawings, such as those shown in Figure 10 and Figure 11, the geometry and materials were created and chosen for this project.

MCNP allows for several different methods of creating geometric inputs. Those selected for this project were planes, rectangular parallelepipeds (RPP), cylinders, and boxes. RPPs must be normal to the x, y, and z axes [20]. Planes were used to define the universe boundary for the simulations. Nearly all walls created for the geometry were created using RPPs. RPPs must be defined by a minimum and maximum x, y, and z value to create a box normal to the axes [20]. The walls of the Low Scatter Laboratory (LSL) labyrinth were created using boxes as these walls are not normal to the axes [20]. Boxes are created by establishing vectors from a specified corner point of the area in the x, y, and z directions [20]. They can be in any direction or angle with respect to the axes [20]. This input method is useful for walls oriented at an angle with respect to the normal axes. The final input selection was the use of cylinders to define the LSL. This laboratory is the neutron calibration laboratory and was built as a circular room to create a more uniform exposure field and minimize scatter. There are four instrument carts moving in unison within the laboratory to further ensure the exposure field experiences uniform scattering (see Figure 9). A cylinder for the outer edge and inner edge of the 3 ft thick concrete shielding wall was created.

Next the materials must be defined. Materials in MCNP are listed with a user defined number, density, and either elemental or isotopic composition by weight, atom fraction, or atom density depending on the needs of the user [20]. The input values chosen for the concrete and air were copied from the most recent MCNP simulation performed for HPIL of only the LSL [31]. According to the aforementioned simulation, the materials were sourced from PNNL-15870 Compendium of Material Composition Data for Radiation Transport Modeling Rev 2. Subsequently, the gypsum wall board material values were selected from PNNL-15870 Compendium of Material Composition Data for Radiation Transport Modeling Rev 2 [30]. All densities for materials were defined as g/cm^3.

Finally, the universe boundary was defined as being 30 cm from the edge of the building on any given side. This definition tells the simulation to ignore anything outside of those boundaries. After the geometry and materials were input correctly, all RPPs, cylinders, and boxes of the same materials were set into a single cell to produce continuous walls and air spaces within the building. This ensured there were no gaps between surfaces to create unintended radiation streaming during the simulation.

3.3 MCNP Verification

This project was supported by INL's Health Physics Instrument Laboratory. As such, the High Performance Computing (HPC) facility was available for use to run the MCNP simulations. The verification of the use of MCNP on the HPC was performed by INL and published in TEV-2944, "Verification and Validation Testing of MCNP and ORIGEN2 Computer Codes for Idaho National Laboratory (INL) High Performance Computing (HPC) Systems" and TEV-3553, "Verification and Validation Testing of MCNP and ORIGEN2 Application" [32, 33]. Test cases are run each time an update is applied to the HPC system to validate the continued use of MCNP on the HPC [32]. Test cases are listed below:

- "3D geometry modeling capabilities that treat arbitrary 3D configurations of materials in geometric cells bounded by first- and second-degree surfaces and fourth-degree elliptical tori" [33]
- "Used for neutron, photon, electron, or coupled neutron/photon/electron transport" [33]
- "Requires the use of either point-wise or group-wise cross-section data, preferably the Evaluated Nuclear Data Files (ENDF) for the International Atomic Energy Agency (IAEA)" [33]

- "For neutrons, all reactions given in a particular cross-section evaluation are accounted for, and thermal neutrons are described by both the free gas and S(alpha, beta) models" [33]
- "For photons, incoherent and coherent scattering must be accounted for and the possibility of fluorescent emission after photoelectric absorption, absorption in pair production with local emission of annihilation radiation and bremsstrahlung" [33]
- "A continuous slowing down model used for electron transport that includes positrons, x-rays, and bremsstrahlung but does not include external or self-induced fields" [33]
- "Output contains numerous tallies: surface and current flux, volume flux, point or ring detectors, particle heating, fission heating, pulse height tallies for energy charge deposition, mesh tallies, and radiography tallies" [33]
- "Software is able to calculate critical eigenvalue of ATR and compute power distribution of ATR fuel elements" [33]

Test cases pertaining to photon transport, 3D geometry modeling, and tally output files pertain to this project and verify the software and computers were operating properly at the time of testing.

3.4 MCNP Experimental Comparison Test Case

To ensure the MCNP simulations were producing reliable results, an experimental comparison test case simulation was created. The experimental comparison test case simulation needed to be a scenario of either known geometry and dose rates or measurable, reproduceable dose rates to compare to the MCNP simulation. A source viewing was chosen as the experimental comparison test case simulation.

Figure 13: Image of 1250 Ci ^{137}Cs source exposed in the source viewing position during the verification assessment. (Image was taken remotely using room cameras)

Source viewing is a process in which the source rabbit is exposed in an acrylic tube to view the integrity of the rabbits (see Figure 4) [14]. This provides an unshielded radiation field, during which, measurements at defined locations can be made. Figure 13 shows the 1250 Ci ^{137}Cs source rabbit in the source viewing exposure tube during the experiment.

Five Mirion RDS-31 meters and five Mirion DMC3000 Electronic Dosimeters were placed in strategic locations around the lab and office areas during an eleven-minute exposure of the 1250 Ci ^{137}Cs source. Data collected from the instruments were compared with the simulation results. All quantifiable error contributors were combined for both the real and simulated data and plotted to visually confirm overlap of values and thereby demonstrated the results of the simulation to be in good agreement.

The MCNP experimental comparison test case input deck defined specific detector points of interest. The detector positions corresponded to the real detector positions measured during the source viewing. The detectors were defined as spheres with 5 cm radii. The area of the simulated

detector was larger than the actual detectors used to increase the volume in which a particle could be detected. Using the actual detector dimensions and volume would have created much more error in the simulation and would have taken significantly longer to produce usable results. Although the actual detectors used in the experiment were not air filled, the MCNP detectors were defined as air spaces.

The choice to fill the detectors with air rather than model the actual detector fill or material is based on how measurements are taken in the field during a project by radiological control technicians (RCTs). RCTs may use a variety of instruments to cover radiological work with differing detectors and materials. Since the purpose of this simulation is to determine safe evacuation zones for a potential real event, the results must be the dose rate in air, not the specific response of the detector used in the experiment. Furthermore, the purpose of the experimental test case simulation was to demonstrate the expanded simulations would result in reasonable results for the geometry and source strength in air filled spaces.

An F4 tally was selected as the desired quantity for the output of the simulation. An F4 tally results in a track length flux average over a cell (particles/cm^2) [20, 23]. The F4 tally was applied to only the detector cells. The source was defined as an isotropic point source with one discrete energy (0.662 MeV) photon. The source strength was input as a FM4, or multiplier, to be applied to the results of the F4 tally. The source strength multiplier was calculated to be in units of particles/hr. Equation 3 below shows how the activity was converted to particles/hr using the activity in curies, conversion between becquerels and curies, photon yield for ^{137}Cs, and the conversion from seconds to hours. The position of the source was set to the source viewing position. The center line of the source capsule was used to define this position (see Figure 6).

$$Source\ Strength\ \left(\frac{particles(\gamma)}{hr}\right) = 785.8\ Ci * \frac{3.7E10\frac{d}{s}}{Ci} * 0.851\frac{\gamma}{d} * \frac{3600\ s}{hr}$$
$$= 8.91E16\frac{particles(\gamma)}{hr}$$

Equation 3

ICRP116 isotropic photon effective dose per fluence conversions were used to convert the cell flux to dose rate via the DE/DF input card. Since the ICRP116 conversion table was in units of pSv·cm^2, a further conversion to rem·cm^2 was required and applied prior to input into the DE/DF cards of the MCNP simulation deck. Table 1 shows the conversion calculations from pSv·cm^2 to rem·cm^2. Only photon energies between 0.01 MeV-1 MeV were included in the conversion inputs.

Energy (MeV)	ISO (pSv·cm^2)	ISO (Sv·cm^2)	ISO (rem·cm^2)
0.01	0.0288	2.88E-14	2.88E-12
0.015	0.056	5.6E-14	5.6E-12
0.02	0.0812	8.12E-14	8.12E-12
0.03	0.127	1.27E-13	1.27E-11
0.04	0.158	1.58E-13	1.58E-11
0.05	0.18	1.8E-13	1.8E-11
0.06	0.199	1.99E-13	1.99E-11
0.07	0.218	2.18E-13	2.18E-11
0.08	0.239	2.39E-13	2.39E-11
0.1	0.287	2.87E-13	2.87E-11
0.15	0.429	4.29E-13	4.29E-11
0.2	0.589	5.89E-13	5.89E-11
0.3	0.932	9.32E-13	9.32E-11
0.4	1.28	1.28E-12	1.28E-10
0.5	1.63	1.63E-12	1.63E-10
0.551	1.67	1.67E-12	1.67E-10
0.6	1.97	1.97E-12	1.97E-10
0.662	2.17	2.17E-12	2.17E-10
0.8	2.62	2.62E-12	2.62E-10
1	3.25	3.25E-12	3.25E-10

Table 1: ICRP116 Dose Conversion Factors from pSv·cm^2 to rem·cm^2 [18]

Since the photon energy for ^{137}Cs is 0.662 MeV, it was not necessary to include photon energies beyond that value. 1 MeV was chosen as an arbitrary upper limit.

When the results of the MCNP experimental comparison test case were produced, the combination of the F4 Tally, FM4 multiplier, and the DE/DF card with ICRP116 dose conversations resulted in units of rem/hr. In this simulation, units of hours were included in the source strength definition to produce the results in rem/hr.

Only photon physics was simulated for all MCNP runs [20]. This selection includes all photoatomic and photonuclear interactions [20]. The MCNP experimental comparison test case simulated 1E11 particles and was processed on the HPC at INL. The run took roughly 5.5 hours to complete. Test runs were completed with between 1E5 and 1E10 both on a desktop computer and on the HPC. By selecting 1E11 particles, the MCNP calculated error was minimized for all detector positions while not taking days to run on the HPC. The results summarized in Section 3.6 Experimental Comparison Test Case Results.

3.5 Instrument Selection

Two instruments were selected to be used during the source viewing: Mirion RDS-31 and Mirion DMC3000 Electronic Dosimeter (ED). The Mirion RDS-31 was selected for its size and similarities to the Thermo Fisher RadEye B20-ER used by RCTs during job coverage at INL. Both the RadEye and the RDS-31 use Geiger-Muller (GM) detectors as the primary detector [28, 34]. The RadEye uses a pancake GM while the RDS-31 uses a compensated cylinder GM tube [28, 34]. The RDS-31 was also selected for the histogram function integrated into the instrument [34]. When the instrument is powered on, it will log measured readings every 10-30 seconds (dependent

on firmware version) [34]. These data can be exported from the instrument in the form of a spreadsheet. The readings can then be analyzed over time for more statistically significant data.

The Mirion DMC3000 is the standard electronic dosimeter used at INL. When a Radiological Work Permit (RWP) requires a worker to wear an electronic dosimeter, the DMC3000 is programed with the specific dose and dose rate alarm settings for the RWP [5, 6, 24].

Figure 14: DMC3000 Electronic Dosimeters (top) and RDS-31 Meters (bottom) used during verification experiment

All work at HPIL requiring the use of the irradiator systems, requires an electronic dosimeter be worn by the worker [5, 6]. While in use, the ED displays a cumulative dose and will alarm if the limits of either dose or dose rate are met [26, 27]. The internal detector is a silicon dioxide detector [29].

The EDs were placed in area of laboratory exits or common workstations for technicians. These areas are not typically surveyed during non-routine operations as the radiation line is not typically near those areas. Some technicians in those work areas would be wearing an ED during a non-routine operation and it would provide a portion of the dose contribution to that worker during that time. The EDs placed near exits were chosen to represent the potential dose for evacuating staff members.

There are two different RWPs approved for use at HPIL: Routine Operations and Non-Routine Operations [5, 6]. Routine operation RWP dose and dose rate alarms are 10 mrem and 50 mrem/hr respectively [5, 6]. The non-routine RWP dose and dose rate alarms are 30 mrem and 100 mrem/hr respectively [5, 6]. These values would be monitored and enforced using the ED worn by the worker.

EDs are only part of the worker dose picture. An OSL is also worn at all times by every worker at HPIL. The combination of ED data, OSL readings, and area dosimeter data determines the dose assigned to the worker annually. Frequently an ED will register a dose and it will not show on the dose report as reportable.

The selected instruments display in units of rem or rem/hr. However, HPIL calibrates all instruments to exposure rate [9]. Because of this, even dose rate instruments are calibrated to an exposure value in roentgen/hr. At INL, it is widely accepted as a factor of conservancy, 1 roentgen equals 1 rem for photons. The actual relationship between the two is 1 roentgen equals 0.869 rem for photons [4]. This value is based off the relationship between exposure in air (roentgen) and dose in rad [3]:

$$D(rad) = \frac{Exposure\ (R) * \left(2.58x10^{-4}\frac{C}{Kg\ R}\right) * \left(33.7\frac{eV}{ip}\right) * \left(1.6x10^{-19}\frac{J}{eV}\right)}{\left(1.69x10^{-19}\frac{C}{ip}\right)}$$

$$D(rad) = 0.869 * Exposure\ (R)$$

Equation 4

The relationship between rad and rem is 1:1 for photons, however the units do not indicate the same information. Rem, or Roentgen Equivalent Man, indicates the dose and the risk from receiving that dose using a quality factor. Rad, or radiation absorbed dose, is simply the absorbed dose in a medium [25]. By assuming the 1:1 relationship between roentgen and rem for photons, there is built in conservancy to all measurements made in the field. This is one of many assumptions or simplifications the radiation protection field uses to ensure conservative protection measures.

3.6 Experimental Comparison Test Case Results

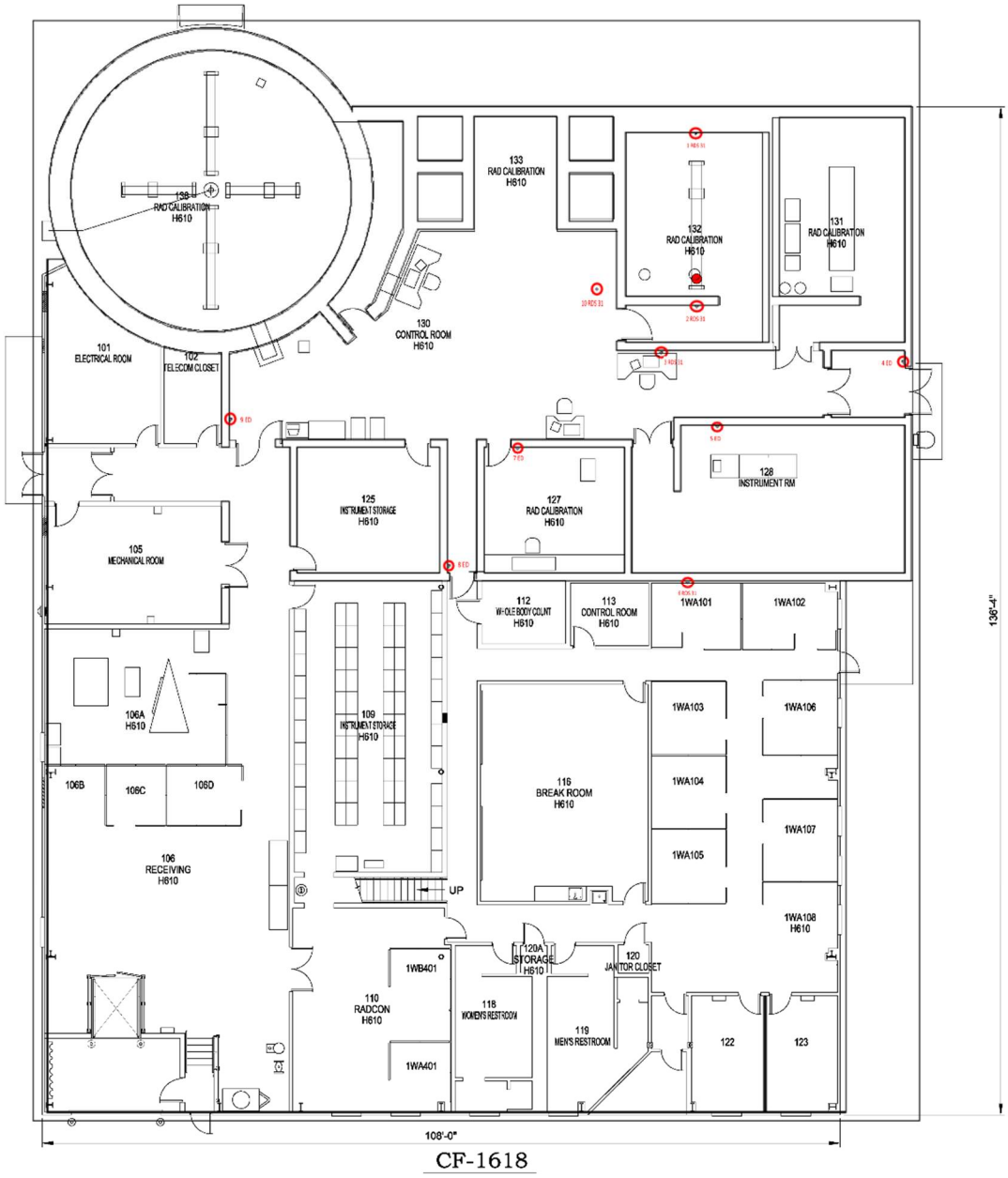

Figure 15. Detector placement for verification test and simulation. Source position is the red dot in Rm 132 [19]

Accounting for the calibration error and standard deviation (σ) in the meter readings, the 95% confidence (±2 σ) interval was determined for each meter. The range was then compared to the MCNP simulation determination with associated error.

	Pos 1	Pos 2	Pos 3	Pos 9	Pos 10
Average Dose Rate (rem/h)	7.191	1.551	6.442E-04	1.636E-03	9.535E-02
2 Sigma Error (actual)	20.1%	20.02%	22.21%	10.00%	31.79%
MCNP Sim. Dose Rate (rem/h)	6.631	1.749	7.737E-04	3.451E-03	1.153E-01
2 Sigma Error (MCNP)	0.0012	0.0018	0.072	0.0372	0.0078
% Diff (Average v MCNP)	7.79%	-12.76%	-20.09%	-110.92%	-20.99%

Table 2: Experimental Detector Actual versus MCNP Detector Results

The source viewing was performed using the largest ^{137}Cs source: decayed activity of 785.8 Ci. The source was raised for 11 minutes, then automatically lowered into a safe position. Detectors and EDs were placed around the lab and office areas as shown on Figure 15. After the exposure ended, the detectors were removed, and data collected. Table 2 shows the results of the source viewing with associated errors and the MCNP results and associated errors. Table 2 also shows the percent difference between the averages of each measurement point.

Table 2 only references five of the ten measurement positions. This is because the meters in positions 4-8 resulted in zero values on the meter and background values for the MCNP simulation. Positions 1 and 2 results were the closest to the actual measurements. These positions reflect either the unshielded dose rate of the ^{137}Cs source or through just one wall of shielding. Position 1's MCNP result was lower than measured. This could be because the equipment in the room was not simulated. The equipment could have increased the scatter in the room and contributed to a higher dose rate being observed.

The actual measurement for Position 2 was higher than MCNP simulated. This could potentially be from slight differences in the building geometry resulting in different scatter results.

The drawings used may not have been exactly what was built. The equipment and storage shelves in the room could have increase the scatter into the labyrinth where the meter was located.

Positions 3 and 10 were within 21% of the actual measurement. Both had the MCNP simulating higher dose rates than measured. When processing the expanded simulation plot for Source Position 1, there was a gradient of dose rate values along the wall of Position 3 was located. Moving the reference point ± 3 m would give you dose rates between 3 mrem/h and 0.5 mrem/h. This variation, again, could be from the potential scatter from objects not included in the MCNP simulation or variations in the building geometry. Another potential for variation in the values is the material chosen for the concrete in the building. The density and composition of the actual concrete may vary slightly from what was input in MCNP.

Position 9 was an ED displaying a dose of 0.3 mrem over the 11-minute exposure. This resulted in an average dose rate of 1.6 mrem/hr. The MCNP simulation produced a value within the same order of magnitude, not within the error range of the measurement, and higher than the observed value. During the exposure, an RCT measured a dose rate around 2.8 mrem/hr in the area of Position 9. This value more closely matches the value seen by the MCNP simulation. Furthermore, a recorded dose of 0.3 mrem on an ED is commonly disregarded as “not reportable” when dose reports are issued at HPIL. The MCNP simulation resulting in a higher dose rate than the actual provides a conservative estimate of the dose rates in the area. Other reasons for the variation on Position 9 could arise from small differences between the drawings used to create the MCNP geometry and the actual construction of the building. There may also be scatter occurring from the laboratory workstations and materials not included in the MCNP simulation. The discrepancy on Position 9 requires more investigation to achieve more accurate simulation results.

Figure 16: Detector measurements versus MCNP simulated detector measurements with error ranges

The set of charts included in Figure 16 visually display the overlap in values between the measured and MCNP simulated values. Considering the above analysis and comparison of values, it has been demonstrated the MCNP simulation produces usable results. The geometry, source strength, materials, physics, and conversion factors used produce statistically similar results to measurements made in the field.

4 RESULTS

4.1 Expanded Simulations Methodology

After the experimental comparison test case simulation was determined to produce usable results, the detectors were removed and replaced by a F4 mesh tally. The conversions and

multiplication factors remained the same. The mesh was defined for 10 cm x 10 cm x 45 cm boxes in the x, y, and z directions respectively. The height of the mesh areas centered on "whole-body" height, between 120 cm and 165 cm. This height was chosen because it represents the whole-body height on the typical person and also indicates the approximate height an RCT would be taking measurements during job coverage.

The source was "placed" in 7 positions, including in the source viewing position, and run in separate simulations. The positions were chosen to mimic the route the source may follow during

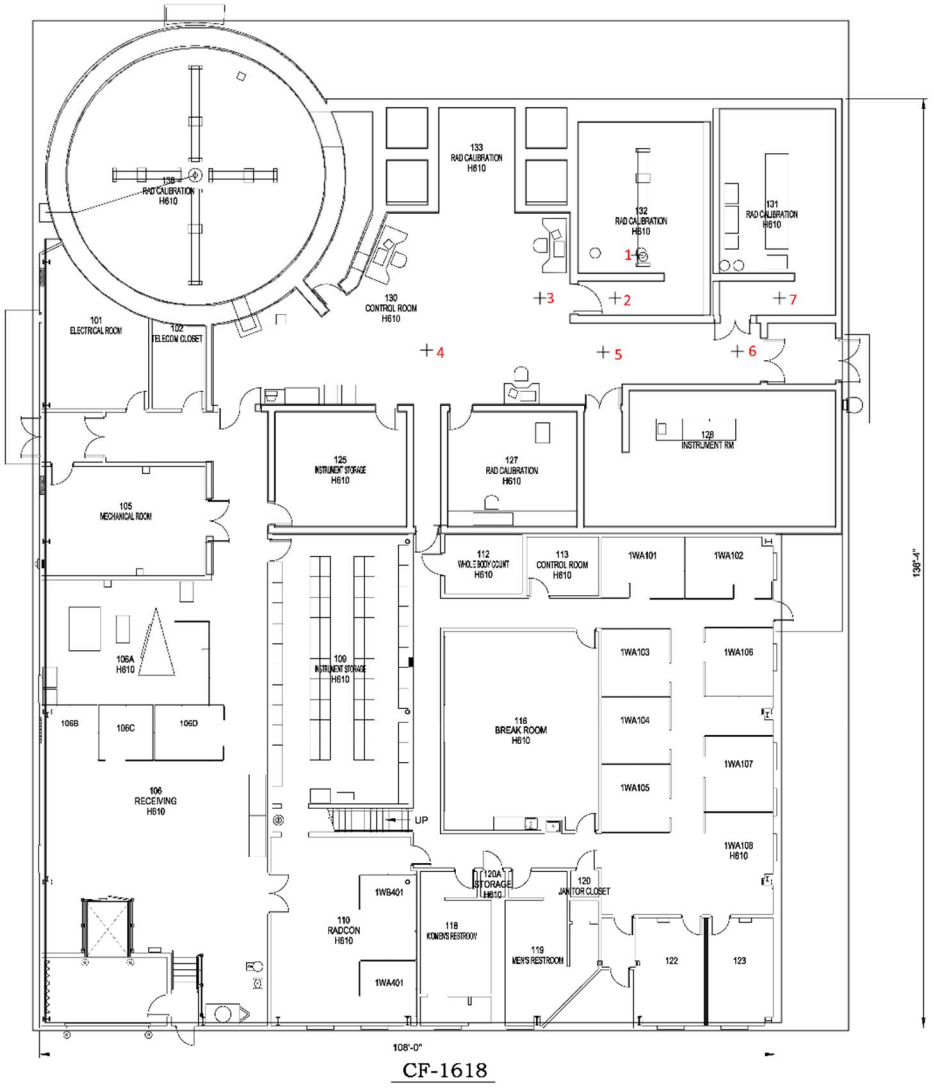

Figure 17: Source placement for expanded MCNP simulations [19]

removal from the GBI room during a non-routine operation. Figure 17 shows the approximate placement of the sources for each MCNP run. If the source were to be removed from the system and not placed in the storage carousel (see Figure 3), it would be placed in a lead transfer shield drawer and wheeled into the X-Ray Beam Laboratory (XBL) for storage. That path accounts for positions 2, 3, 5, 6, and 7. Position 4 was chosen to show the worst potential position for the source to be uncontrolled due to the lack of shielding when in direct line with the exit hallway.

Every position, other than Position 1, the source is laying on its side on the floor. Based on the measurements provided in Figure 7 and Figure 8, the point source is placed about 2 cm off the ground. The source position meshes simulated 1E11 particles and was processed on the HPC cluster at INL. Each run took roughly 5.5 hours to complete. All source position meshes were then plotted using the Plot Window function for MCNP. A plot for dose rates, INL radiological postings, and error was produced for each position. All plots can be seen in Appendix A.

4.2 Expanded Simulation Results

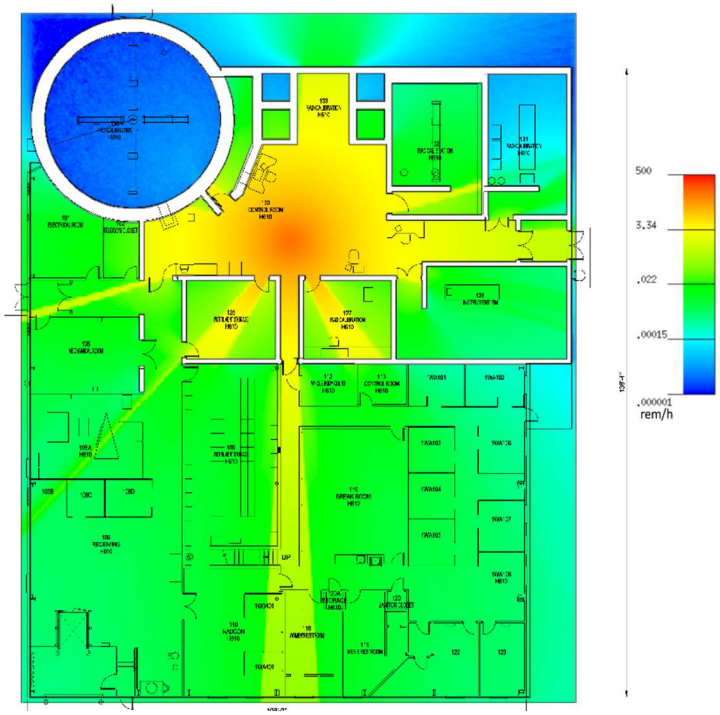

Figure 18: Source Position 4 dose rate heat map (rem/h) (also Figure 32 in Appendix A)

From the plots generated for each source position, Positions 4 and 5 have the highest dose rates and furthest reach into the front half of the HPIL building. This is to be expected as these positions align the source with the least amount of shielding between the front and back halves of the building. Figure 18 shows the dose rate heat map for source Position 4 in rem/hr. This plot shows the graded radiation stream coming out of the hallway and exiting the building (starting with dark yellow and dissipating to yellowish-green). It can be seen by this plot, there may be safe evacuation zones in the front corners of the building and down the left side of the building for this scenario.

Since this project was developed for the use of HPIL at INL, another useful representation of the data is to filter the dose rates by the corresponding radiological hazard posting requirements.

INL is under the Department of Energy and must adhere to the regulations of 10 CFR 835 "Occupational Radiation Protection" and the associated DOE guide "DOE G 441.1-1C" [1, 7, 24]. Using those two documents, the INL Radiological Controls Manual was developed. All three of these documents explain the use of postings to make workers aware of the hazards in work zones and requirements for entry or exit. Table 3 defines the relevant radiological postings [24].

Controlled Area	Radiation Area	High Radiation Area	Very High Radiation Area
<100 mrem/yr	> 5mrem/h	>100 mrem/h	>500 rad/h

Table 3: Radiological posting definitions [1, 7, 24]

Figure 19: Source position 4 Radiological Postings map

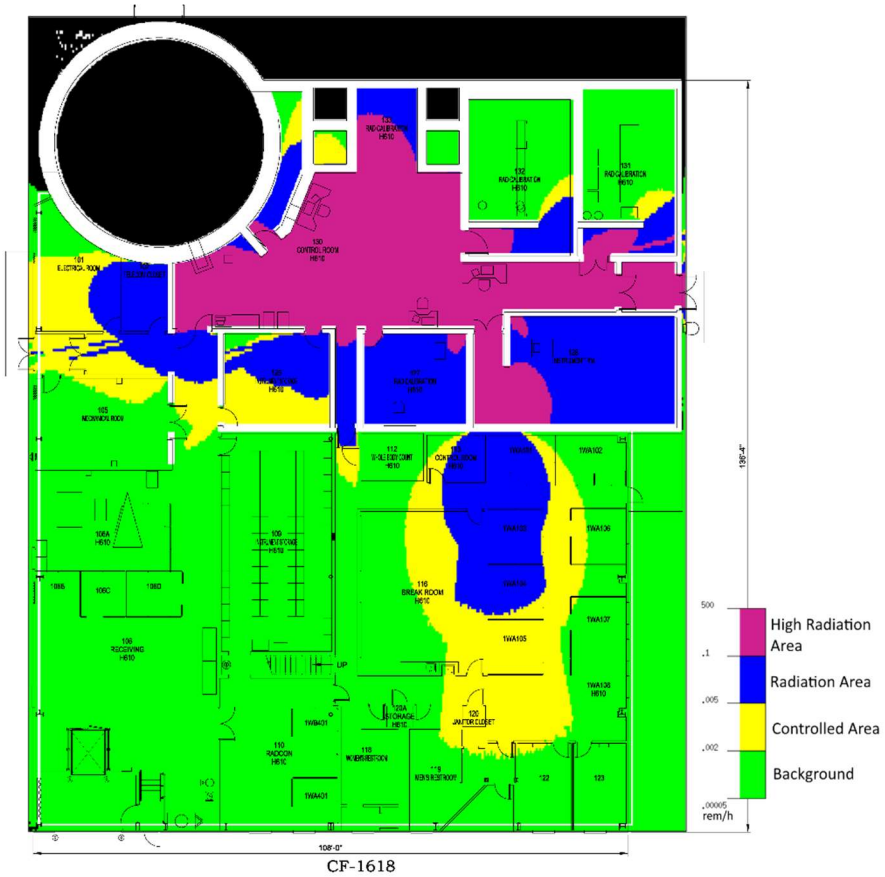

Figure 20: Source Position 5 Radiological Postings map

Source Position 4 would create the need for a High Radiation Area and Radiation Area to be posted to the front of the building and possibly into the parking lot, as shown in Figure 19. When investigating the values on the furthest reaches of the High Radiation and Radiation Areas for Position 4, the dose rates drastically drop off near the edge of the building and may not extend much past the sidewalk outside the building.

Position 5 also produces a radiation area in a large portion of the front offices. Figure 20 shows an intrusion into the office spaces on the right side of the building. Safe zones for this scenario are primarily on the left-front side of the building.

Both Position 4 and 5 are the worst-case scenarios in terms of source position. However, they are not the most probable locations for an uncontrolled source. Positions 2, 3, and 7 are more likely

because of the actions being taken in those two areas of the pathway. Position 2 is around the first turn the cart would make. Position 3 represents the turn needed to walk down the hallway towards

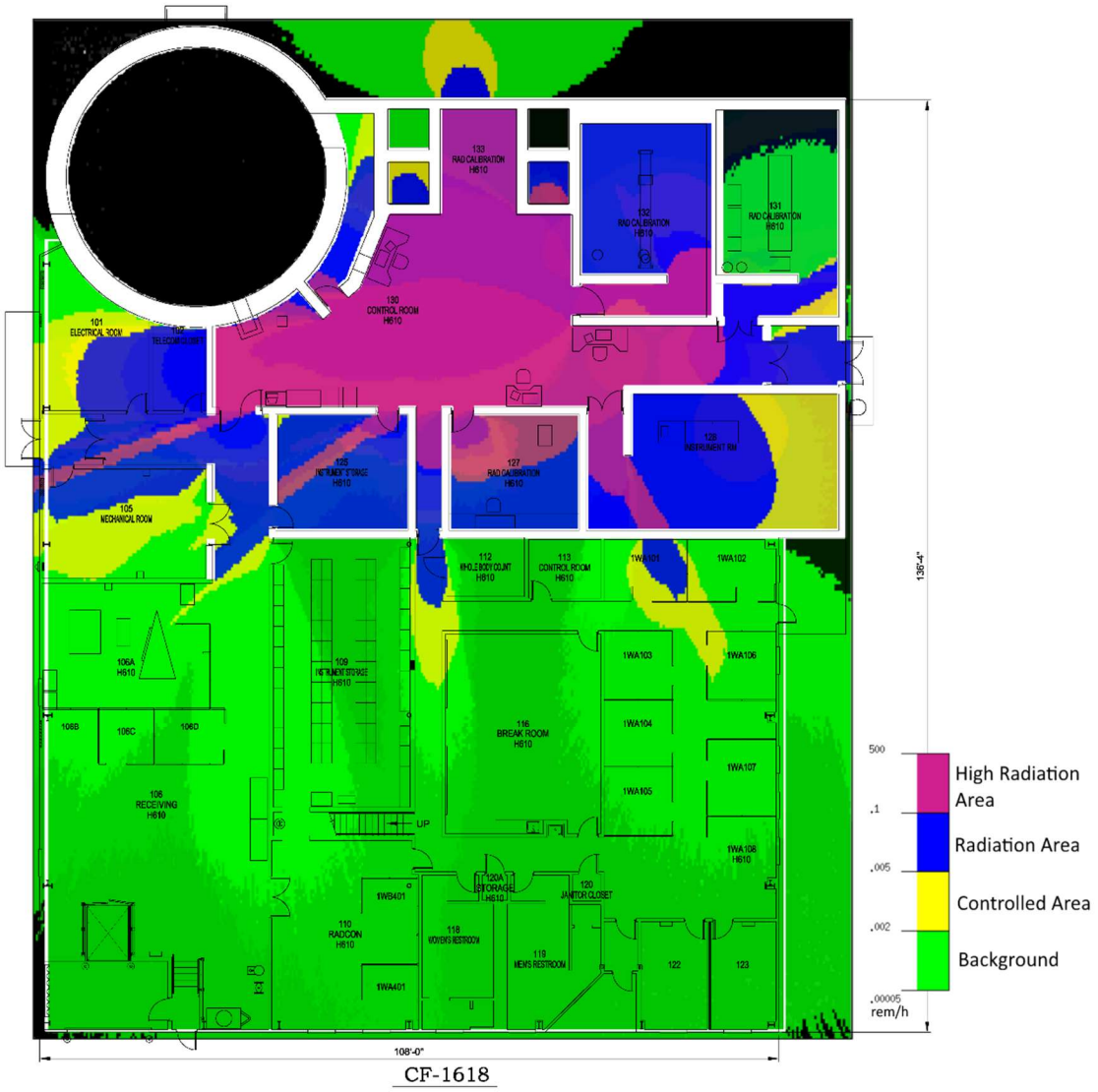

Figure 21: Overlay of source positions 1, 2, 3, 6, and 7 to show save zones

the XBL, and Position 7 represents the area the cart passes over a floor cable run (bump in the floor). These are the most likely positions and movements to produce an inadvertent action resulting in an uncontrolled source.

With that in mind, an overlay of the remaining source positions was created to show the area of the building considered safe for evacuation. Figure 21 shows shallow parturitions of Radiation Areas into the office areas near the lab exit and in line with the instrument repair shop entrance.

Using Figure 21, a general statement can be made; so long as staff evacuate to the front portion of the office area or loading bay, in most situations, the dose rates would be sufficiently low and would not warrant a complete building evacuation.

5 CONCLUSION

The purpose of this project was to create an MCNP simulation capable of producing usable results for the HPIL in the event of an uncontrolled source to determine safe evacuation zones. The MCNP simulation created can produce usable results, as demonstrated by the experimental

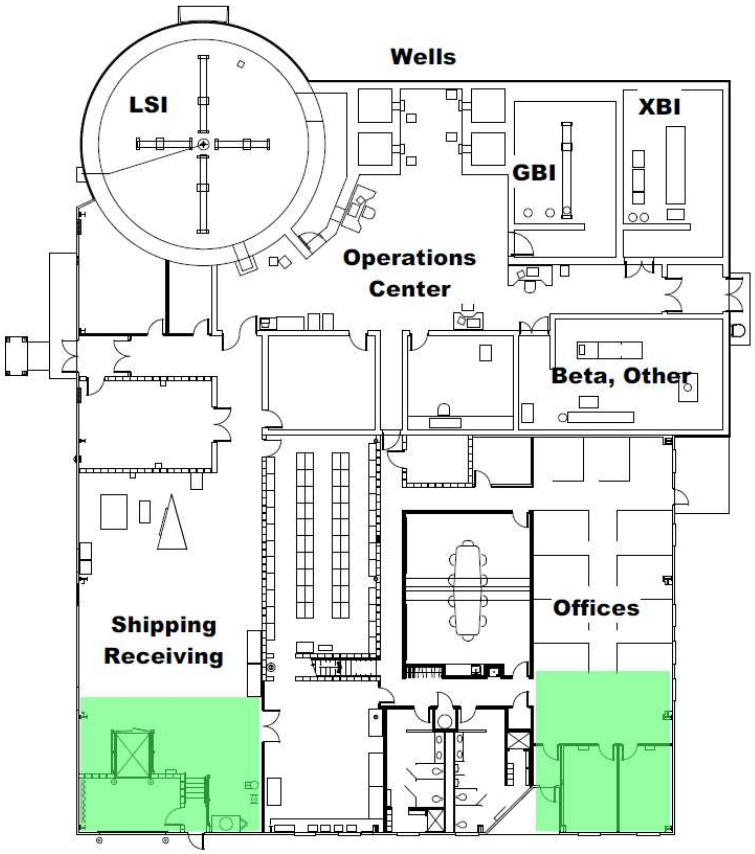

Figure 22: HPIL Safe evacuation zones as determined by MCNP simulations [11]

comparison test case. Using this simulation to model a variety of source positions, safe evacuation zones exist for all scenarios in the front portion of the building.

Figure 22 shows safe evacuation zones (green) for each of the seven source positions. Depending on the source location, the safe evacuation zone can expand to include other areas of the front office and shipping/receiving areas of the building.

If future simulations demand more precision, investigations into sources of scatter within the building would need to be made and accounted for in the MCNP simulation. Some simplifications in the building geometry would need to be adjusted to be more representative of the actual building geometry. New measurements may need to be taken of the building to compare to the drawings used for this simulation. There may be variations in the proposed drawings and the actual building construction contributing to the discrepancies in the data. Including the cinder block walls in the geometry would better focus the radiation stream coming out of the laboratory exit hallway, however investigation into the fill materials would need to be made.

Overall, the simulation was successful and can be used for radiological protection determinations during non-routine operations. Nothing can replace real measurements, but this simulation can inform pre-job decisions and better prepare staff for the unlikely event of an uncontrolled source.

6 REFERENCES

1. 10 CFR 835, Title 10, "Energy," Part 835, "Occupational Radiation Protection," Code of Federal Regulations.
2. ANSI N323AB-2013, "American National Standard for Radiation Protection Instrumentation Test and Calibration, Portable Survey Instruments," American National Standards Institute.
3. Brey, Richard R. *"Dosimetric Quantities",* External Dosimetry, Idaho State University, Pocatello, Idaho. August 2022.
4. Cember, Herman, and Thomas E. Johnson. *Introduction to Health Physics, Fourth Edition*. New York: McGraw-Hill Education, 2008.
5. CFA2022002, 2022, *HPIL Non-Routine Maintenance/Trouble Shooting/Repair of the AIS RGDs,* Idaho National Laboratory, Idaho Falls, Idaho.
6. CFA2022004, 2022, *HPIL Routine Source Handling AIS RGD Operation Activities,* Idaho National Laboratory, Idaho Falls, Idaho.
7. DOE G 441.1-1C, 2008, "Radiation Protection Programs Guide for Use with Title 10 Code of Federal Regulations, Part 835, Occupational Radiation Protection".
8. ECAR-272, 2023, *Characterization of Calibration Fields in the Gamma Beam Laboratory of the HPIL,* Idaho National Laboratory, Idaho Falls, Idaho.
9. ECAR-384, 2009, *Verification and Validation of the Analysis Worksheet for the Calibration of Gamma Radiation Fields at the HPIL*, Idaho National Laboratory, Idaho Falls, Idaho.
10. Forster III, Robert Arthur, Rising, Michael Evan, and Sood, Avneet. The History of Monte Carlo and MCNP at Los Alamos [Slides]. United States: N. p., 2021. Web. doi:10.2172/1898112.
11. Hopewell Designs, INC. *"INL Bldg Floorplan Overall",* February 21, 2023.
12. Hopewell Designs, INC. "*INEEL-M1787 R4: Gamma Beam Irradiator Room Layout Plan View",* February 21, 2023.
13. Hopewell Designs, INC. *"INEEL-M1846 R5: INEEL Irradiator System Overall Equipment Layout",* February 21, 2023.
14. Hopewell Designs, INC. *"M3274 R1: INL Source Viewing Station Overall",* February 21, 2023.
15. Hopewell Designs, INC. *"M4050 R0: GBI Shock Absorber Retrofit",* February 21, 2023.
16. Hopewell Designs, INC. *"M5859 R0: 2in Rabbit for R6050 Source Capsule",* February 21, 2023.
17. ICRP, 2008. Nuclear Decay Data for Dosimetric Calculations. ICRP Publication 107. Ann. ICRP 38 (3).
18. ICRP, 2010. Conversion Coefficients for Radiological Protection Quantities for External Radiation Exposures. ICRP Publication 116, Ann. ICRP 40(2–5).
19. INEEL. *"CFA Health Physics Instrument Laboratory (HPIL)",* May 15, 2000.
20. J. A. Kulesza, T. R. Adams, J. C. Armstrong, S. R. Bolding, F. B. Brown, J. S. Bull, T. P. Burke, A. R. Clark, R. A. Forster, III, J. F. Giron, A. S. Grieve, C. J. Josey, R. L. Martz, G. W. McKinney, E. J. Pearson, M. E. Rising, C. J. Solomon, Jr., S. Swaminarayan, T. J. Trahan, S. C. Wilson, and A. J. Zukaitis, "MCNP® Code Version 6.3.0 Theory & User Manual," Los Alamos National Laboratory, Los Alamos, NM, USA, Tech. Rep. LA-UR-22-30006, Rev. 1, Sep. 2022.

21. Johnson, Thomas E., and Brian K. Birky. *Health physics and radiological health*. Lippincott Williams & Wilkins, 2012.
22. LI-15016, 2018, *Operation of the HPIL Gamma Beam and Low Scatter Irradiator,* Idaho National Laboratory, Idaho Falls, Idaho.
23. Los Alamos National Laboratory. "*Tallies: An Introduction",* Introduction to MCNP6, November 2020.
24. LRD-15001, 2019, *Radiological Control Manual Chapter 2—Radiological Standards,* Idaho National Laboratory, Idaho Falls, Idaho.
25. Martin, James E. *Physics for Radiation Protection: a handbook*. John Wiley & Sons, 2006.
26. Mirion Technologies—Health Physics Division, *DMC 3000 Quick User's Guide,* 2022.
27. Mirion Technologies—Health Physics Division, *DMC 3000 User's Guide,* 2022.
28. Mirion Technologies—Health Physics Division. *RDS-31 S/R Multi-purpose Survey Meter User Manual,* March 24, 2014.
29. P. Martin, Y. Raffray, O. Gaudin, B. Fremy. *"Type tests in compliance with Type Test Program 138385",* MGP Instruments. July 31, 2012.
30. PNNL-15870, Rev. 2, 2021, *Compendium of Material Composition Data for Radiation Transport Modeling,* Pacific Northwest National Laboratory, Richland, Washington.
31. Scates, Wade. *HPIL Template File (Wade Scates)*. MCNP Input Deck. Sept 2022.
32. TEV-2944, 2021, *Verification and Validation Testing of MCNP and ORIGEN2 Computer Codes for Idaho National Laboratory (INL) High Performance Computing (HPC) Systems,* Idaho National Laboratory, Idaho Falls, Idaho.
33. TEV-3553, *Verification and Validation Testing of MCNP and ORIGEN2 Applications,* Idaho National Laboratory, Idaho Falls, Idaho.
34. Thermo Fisher Scientific. *RadEye Selection Guide,* August 2012.

Appendix A –Mesh Plots

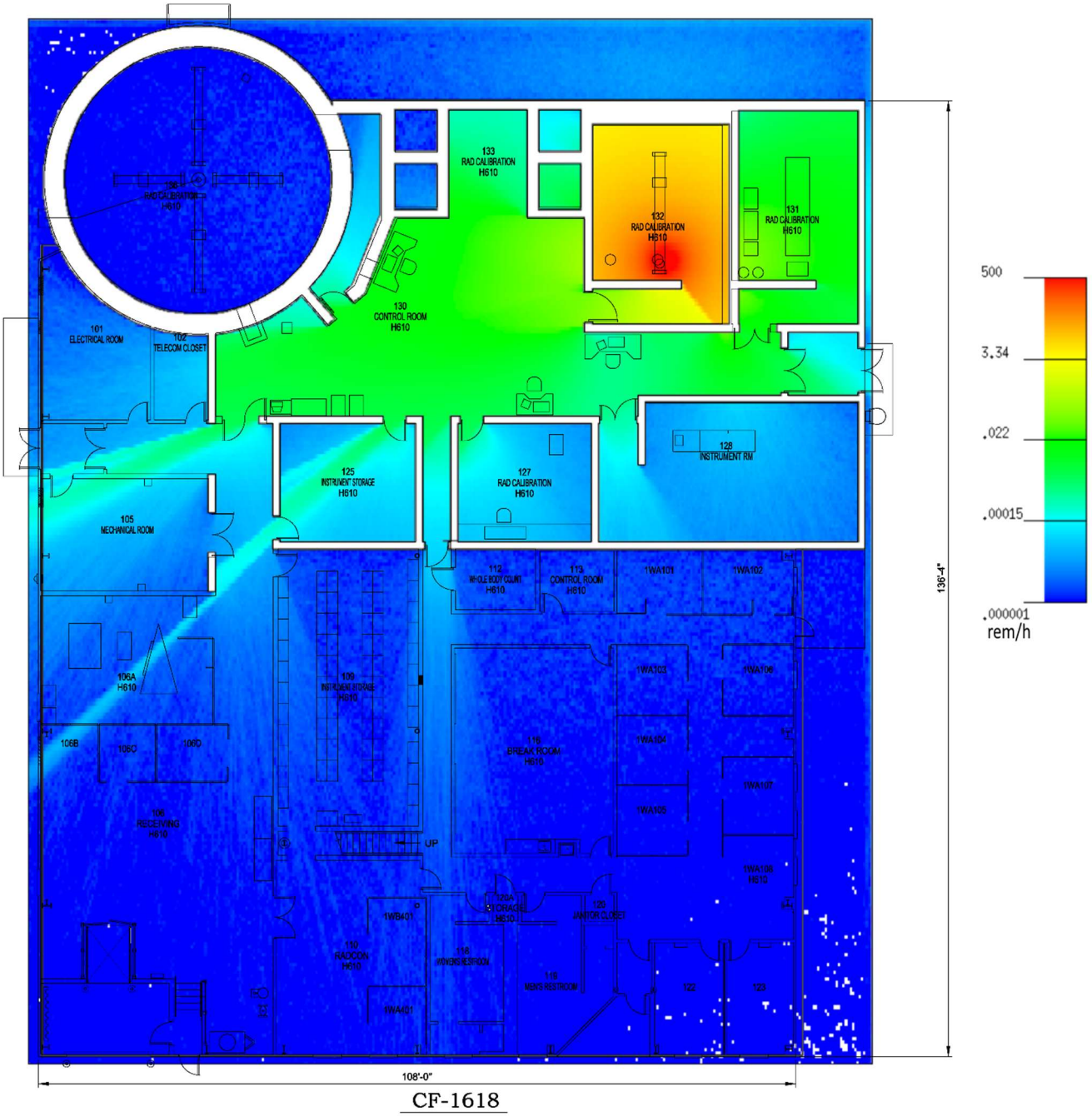

Figure 23: Source Position 1 Dose Rate (rem/h) Mesh

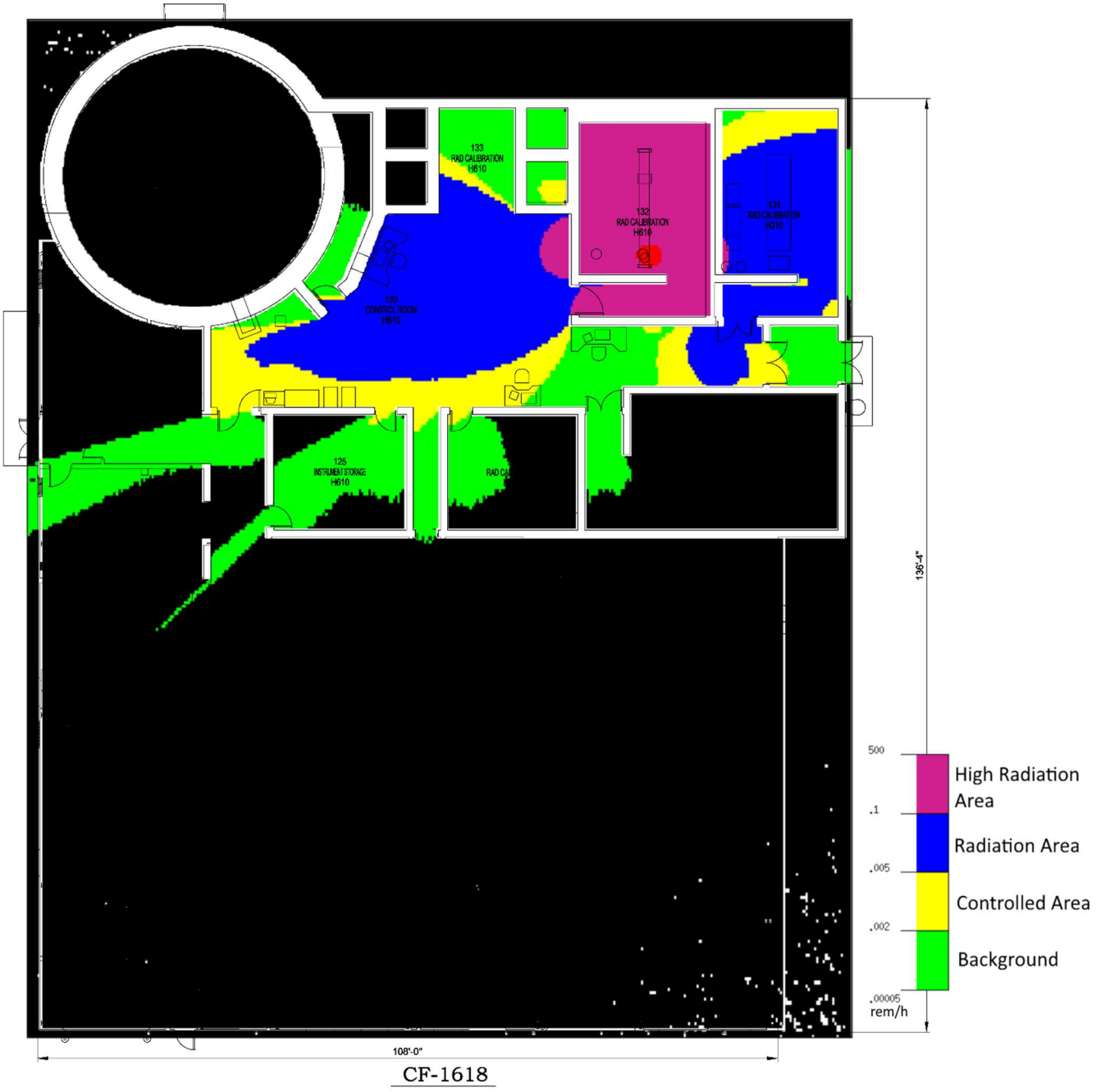

Figure 24: Radiation posting zones Source Position 1

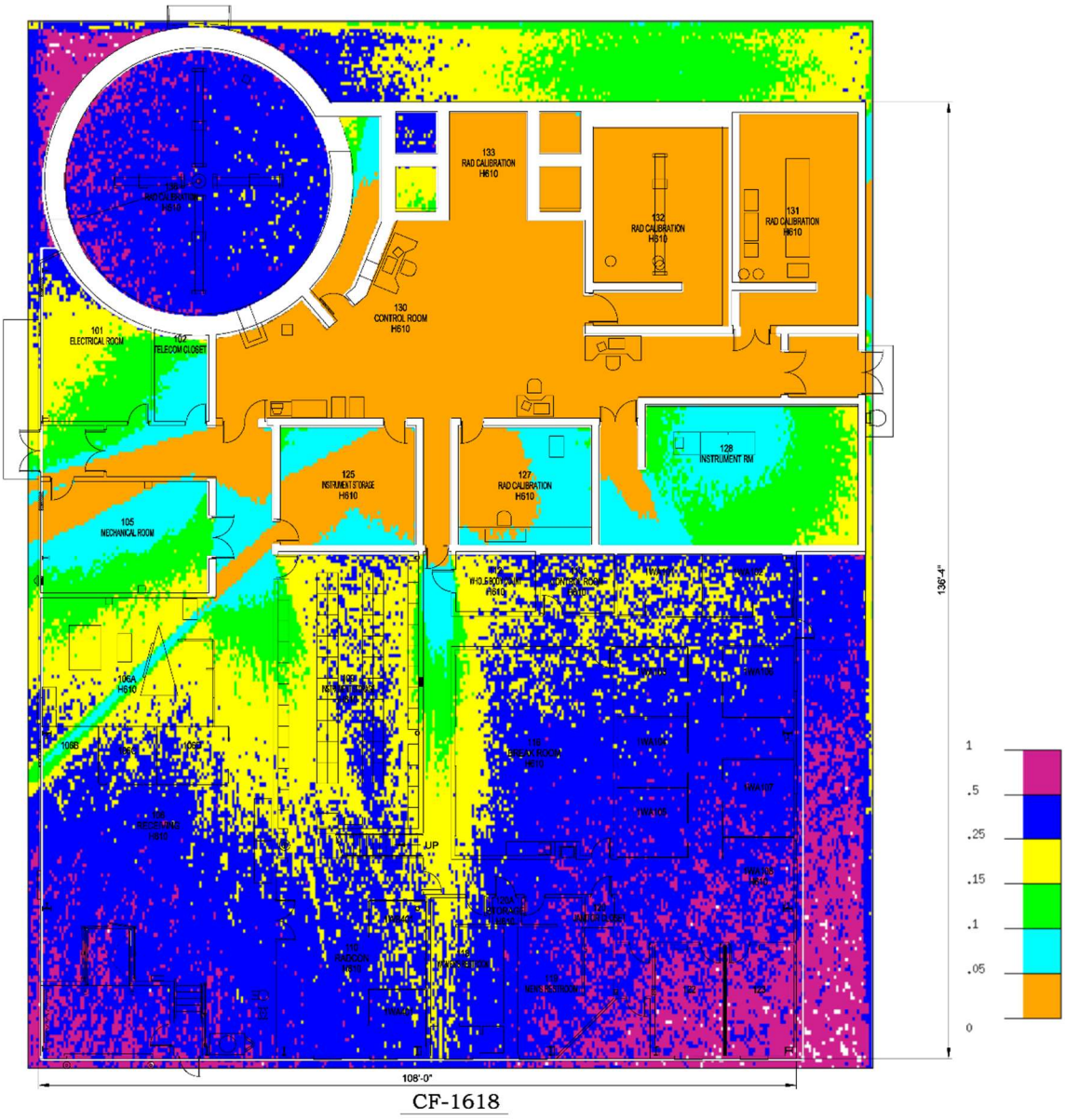

Figure 25: Source Position 1 Dose Rate Mesh Error Plot

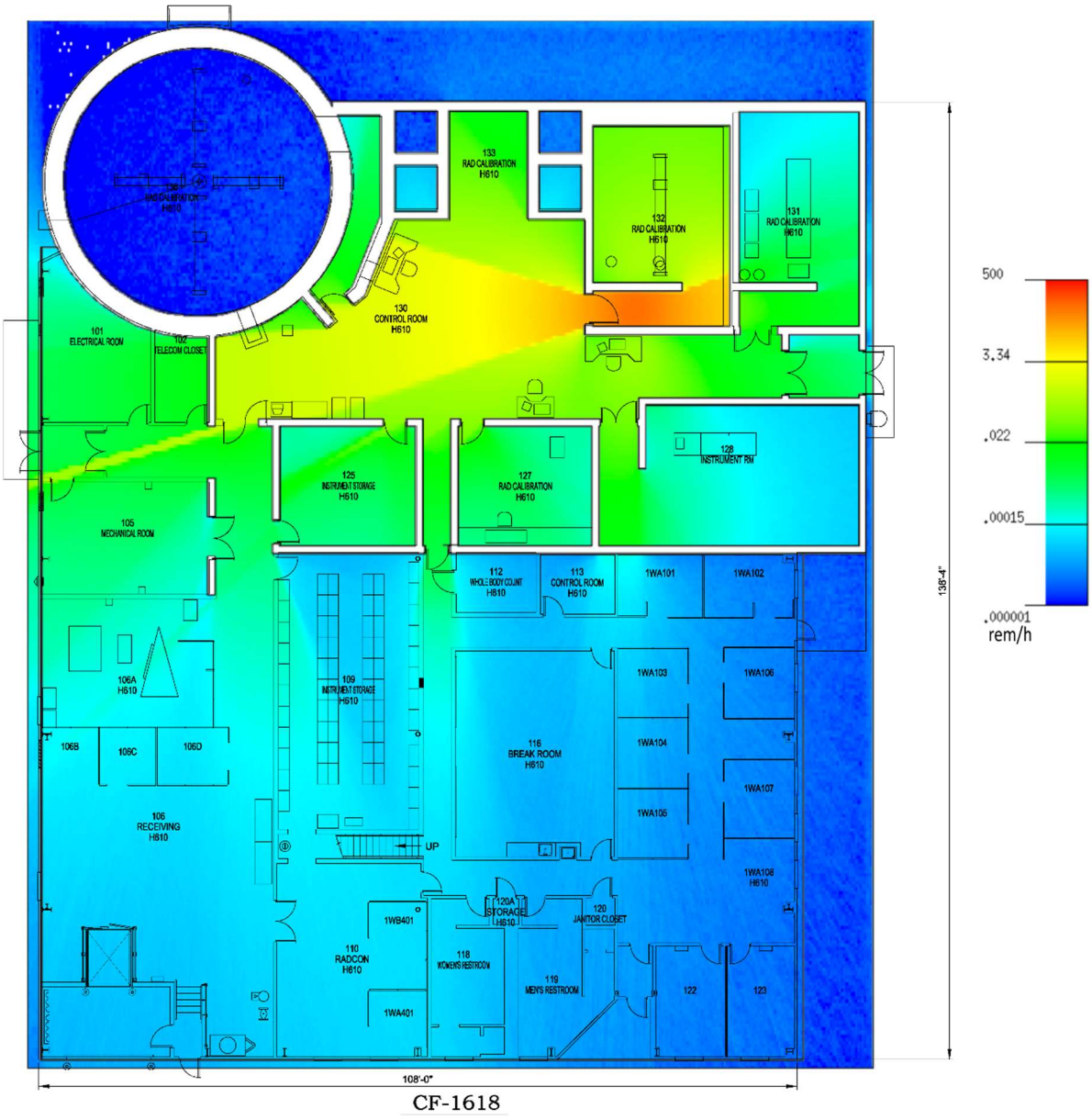

Figure 26: Source Position 2 Dose Rate (rem/h) Mesh

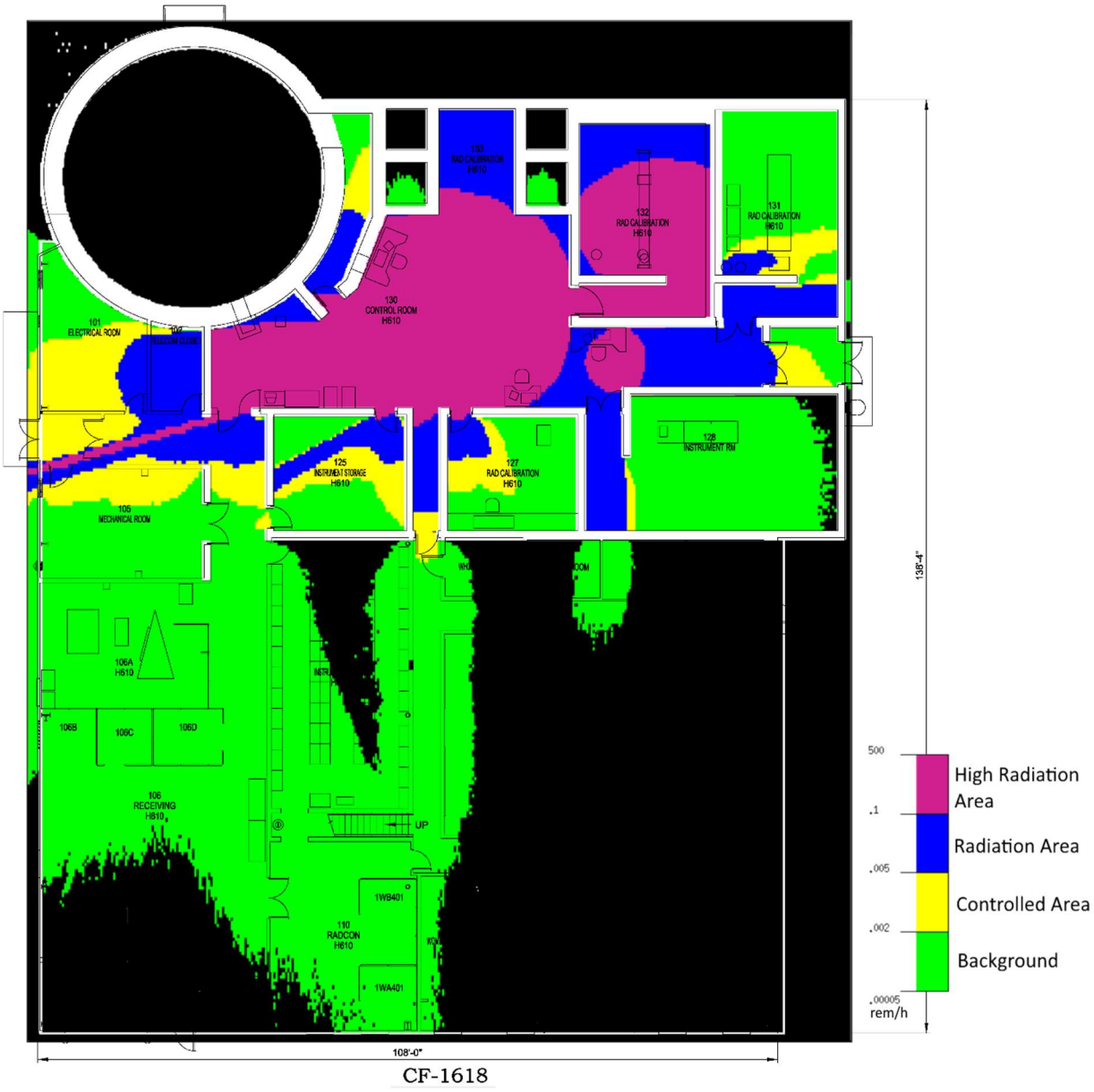

Figure 27: Radiation posting zones Source Position 2

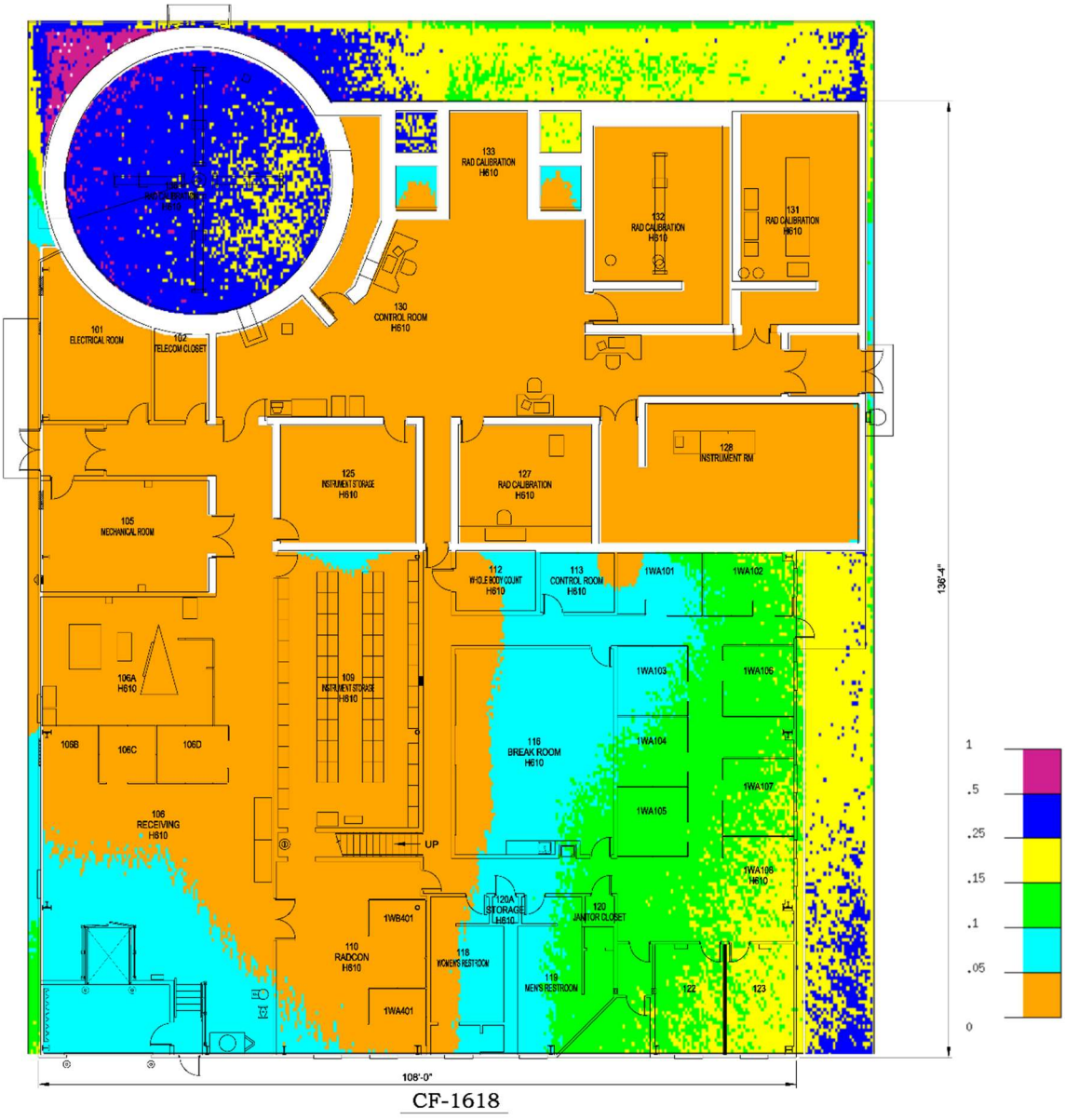

Figure 28: Source Position 2 Dose Rate Mesh Error Plot

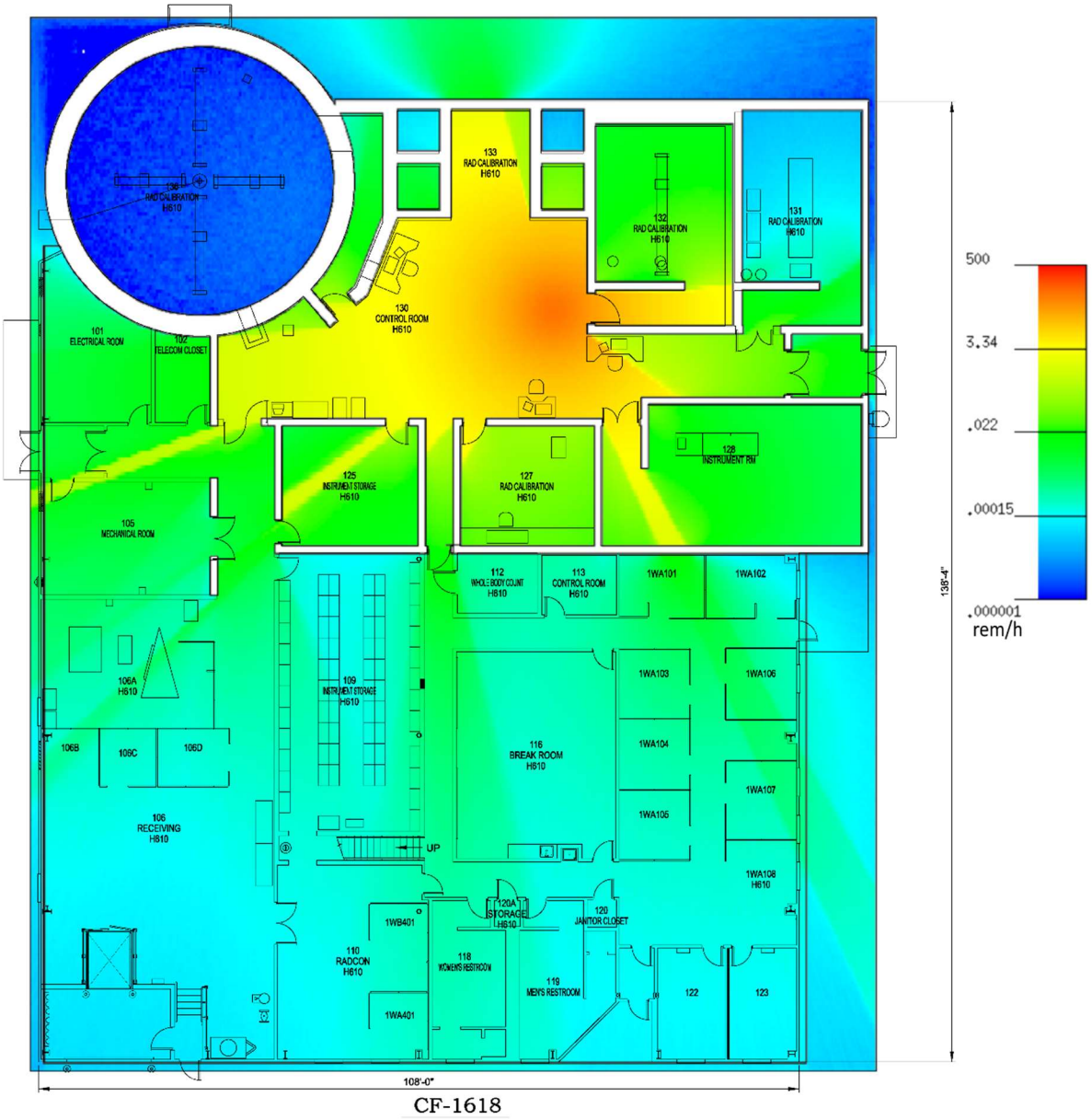

Figure 29: Source Position 3 Dose Rate (rem/h) Mesh

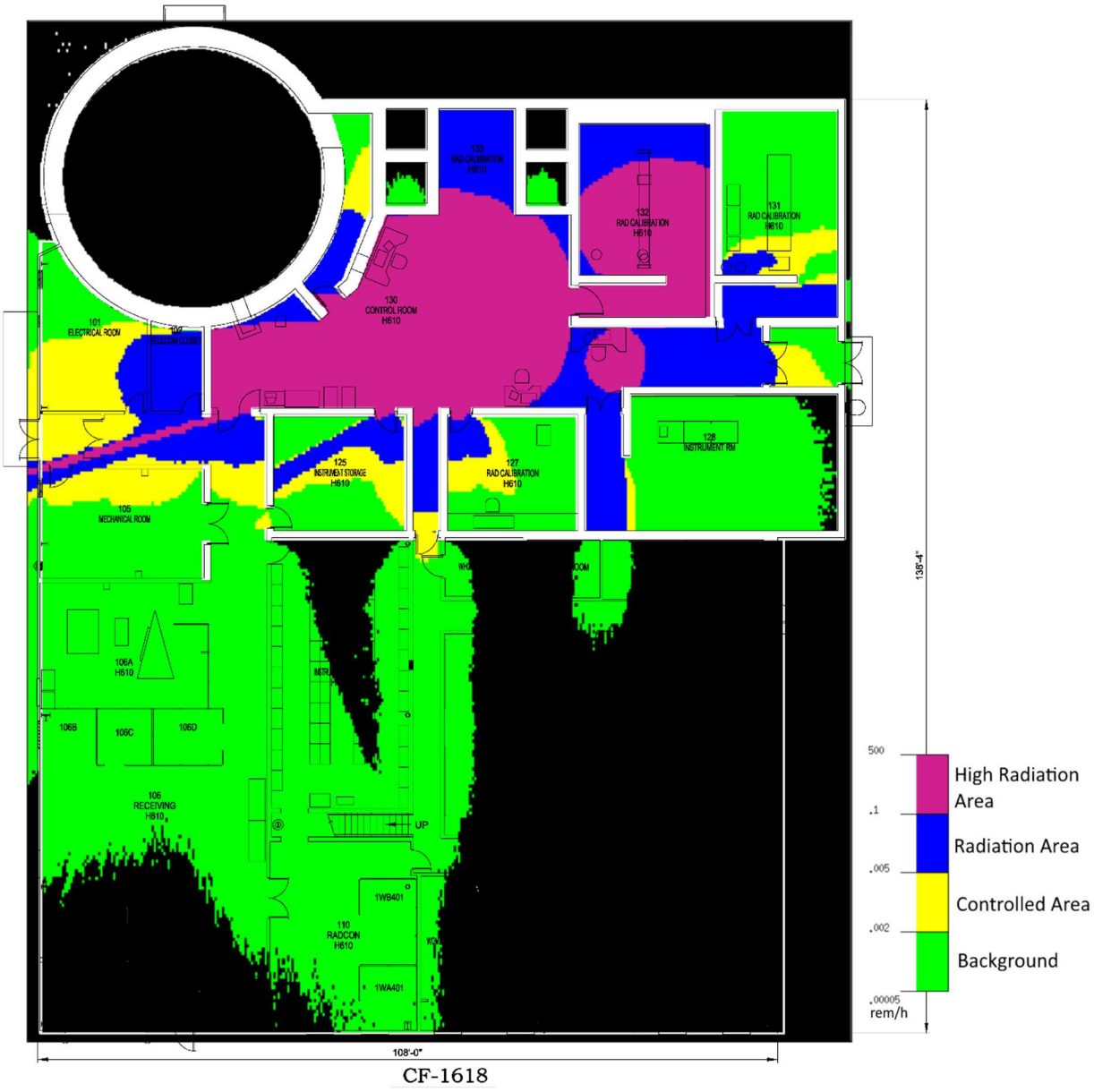

Figure 30: Radiation posting zones Source Position 3

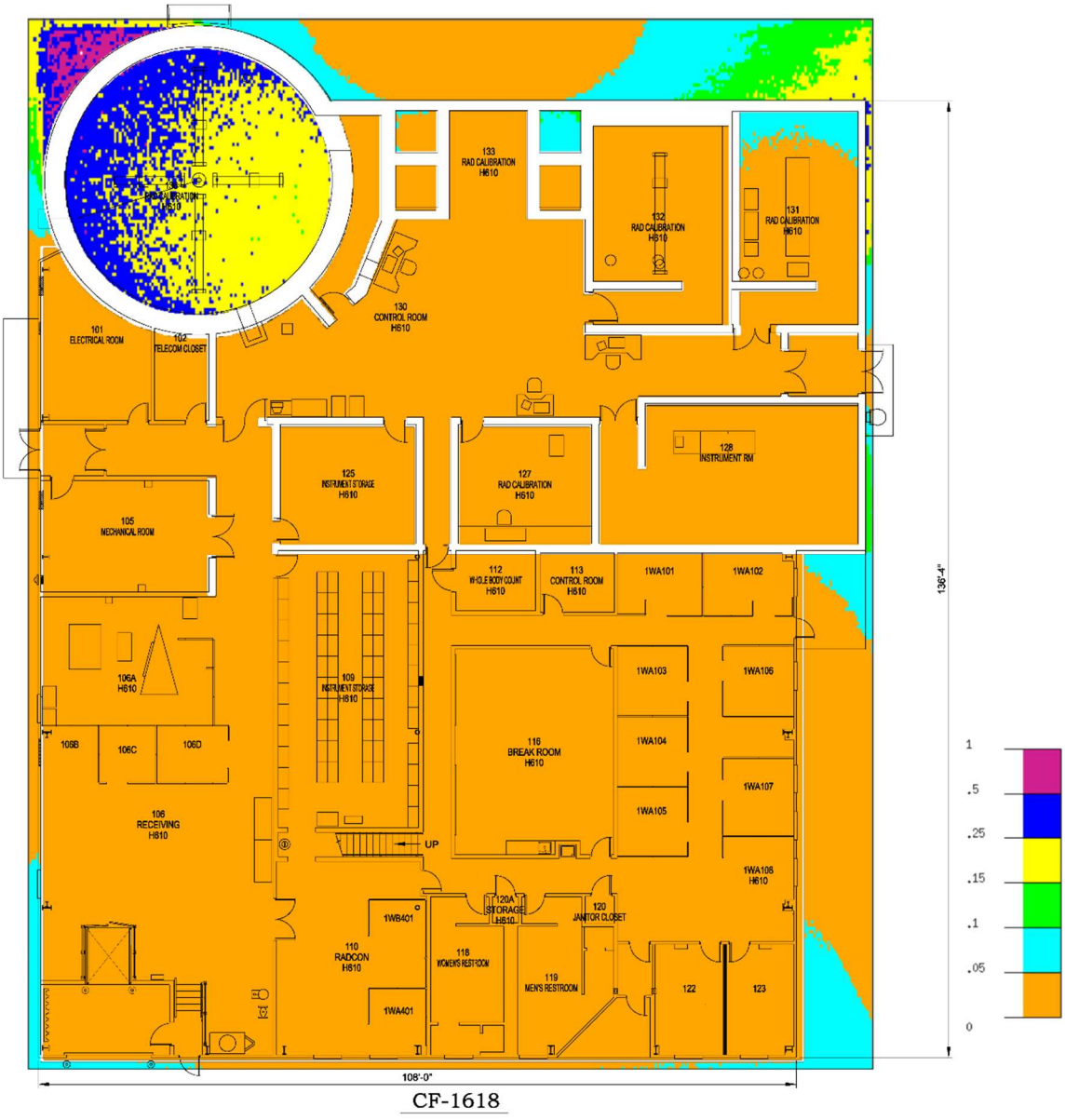

Figure 31: Source Position 3 Dose Rate Mesh Error Plot

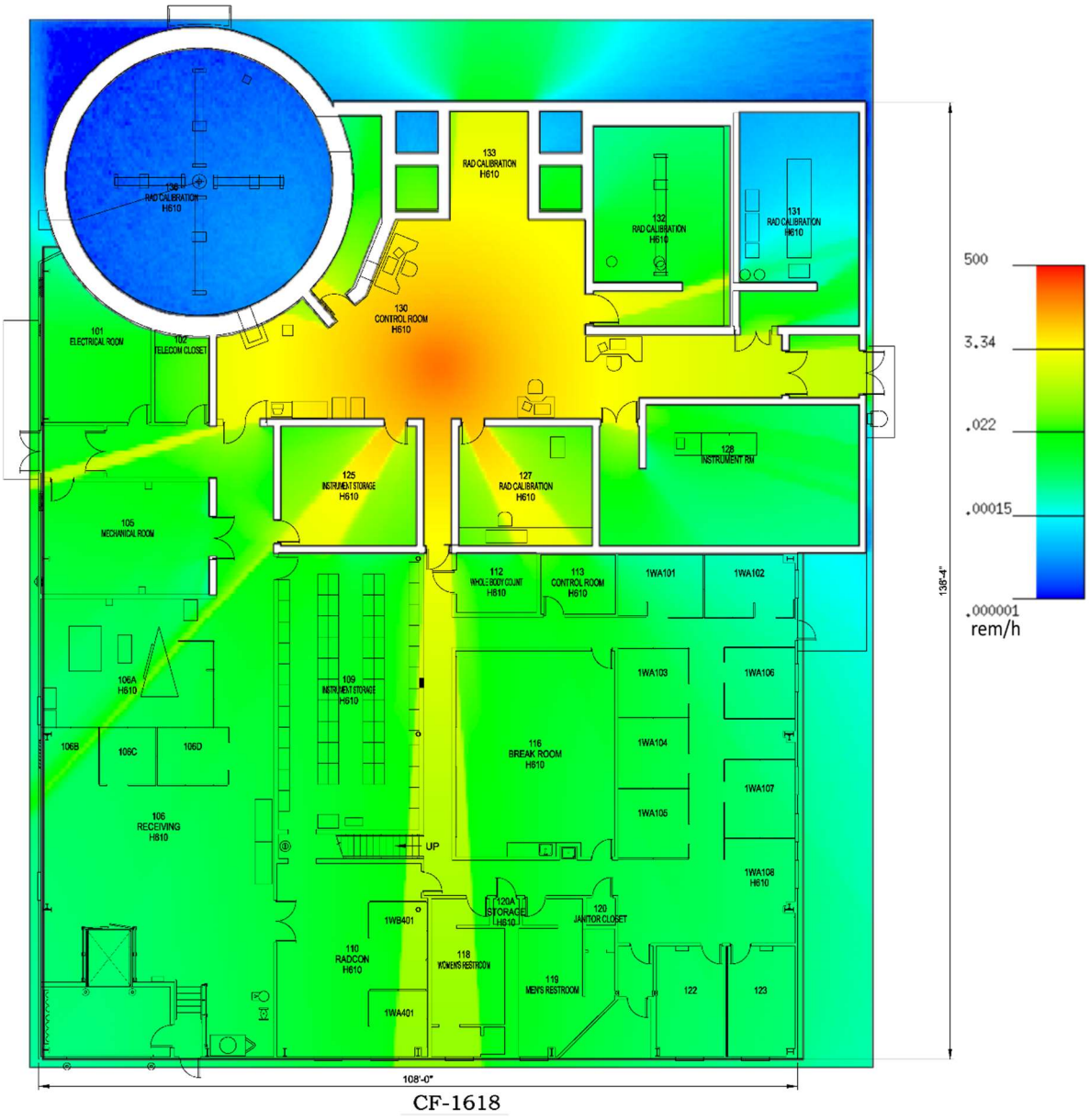

Figure 32: Source Position 4 Dose Rate (rem/h) Mesh

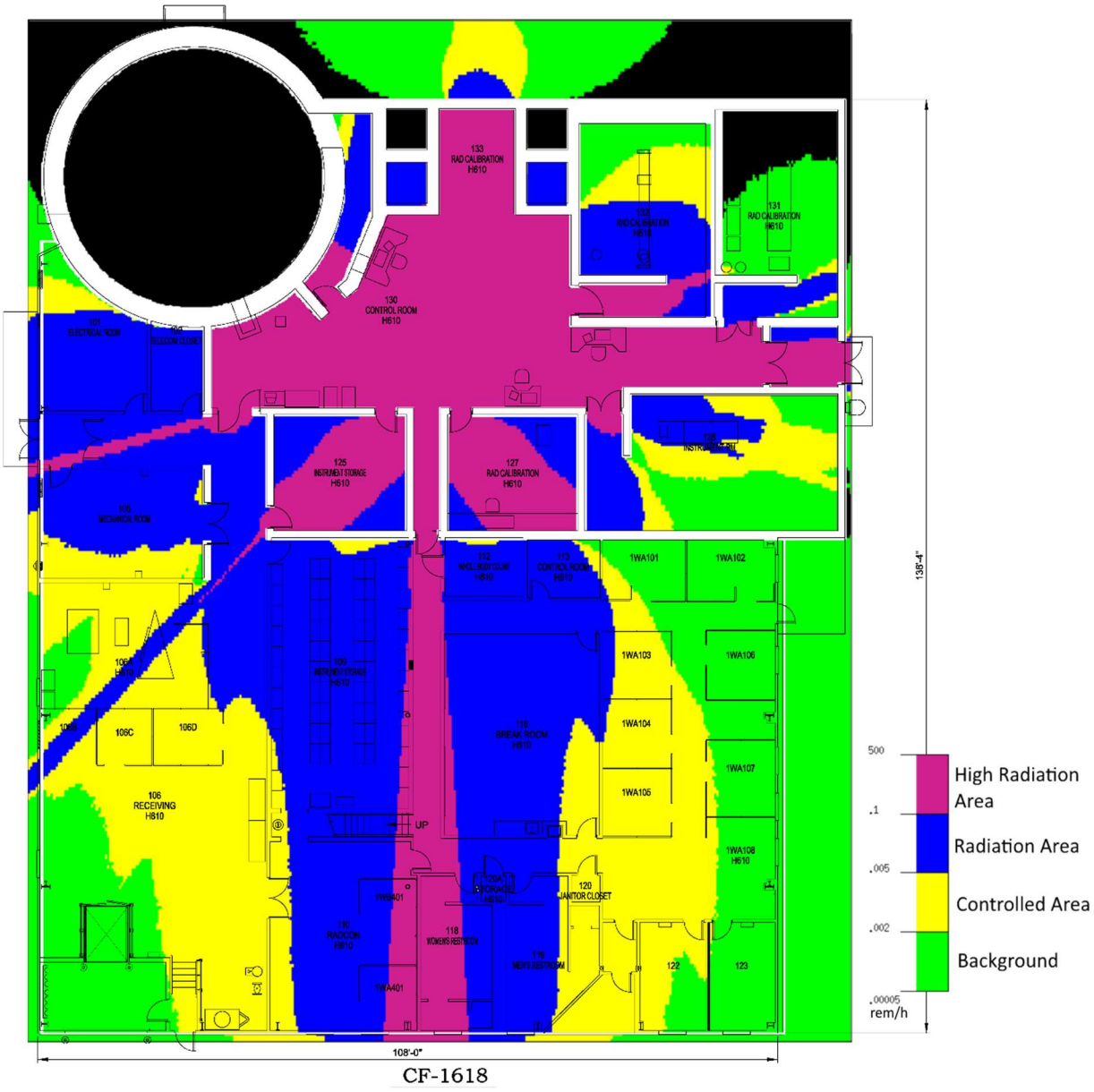

Figure 33: Radiation posting zones Source Position 4

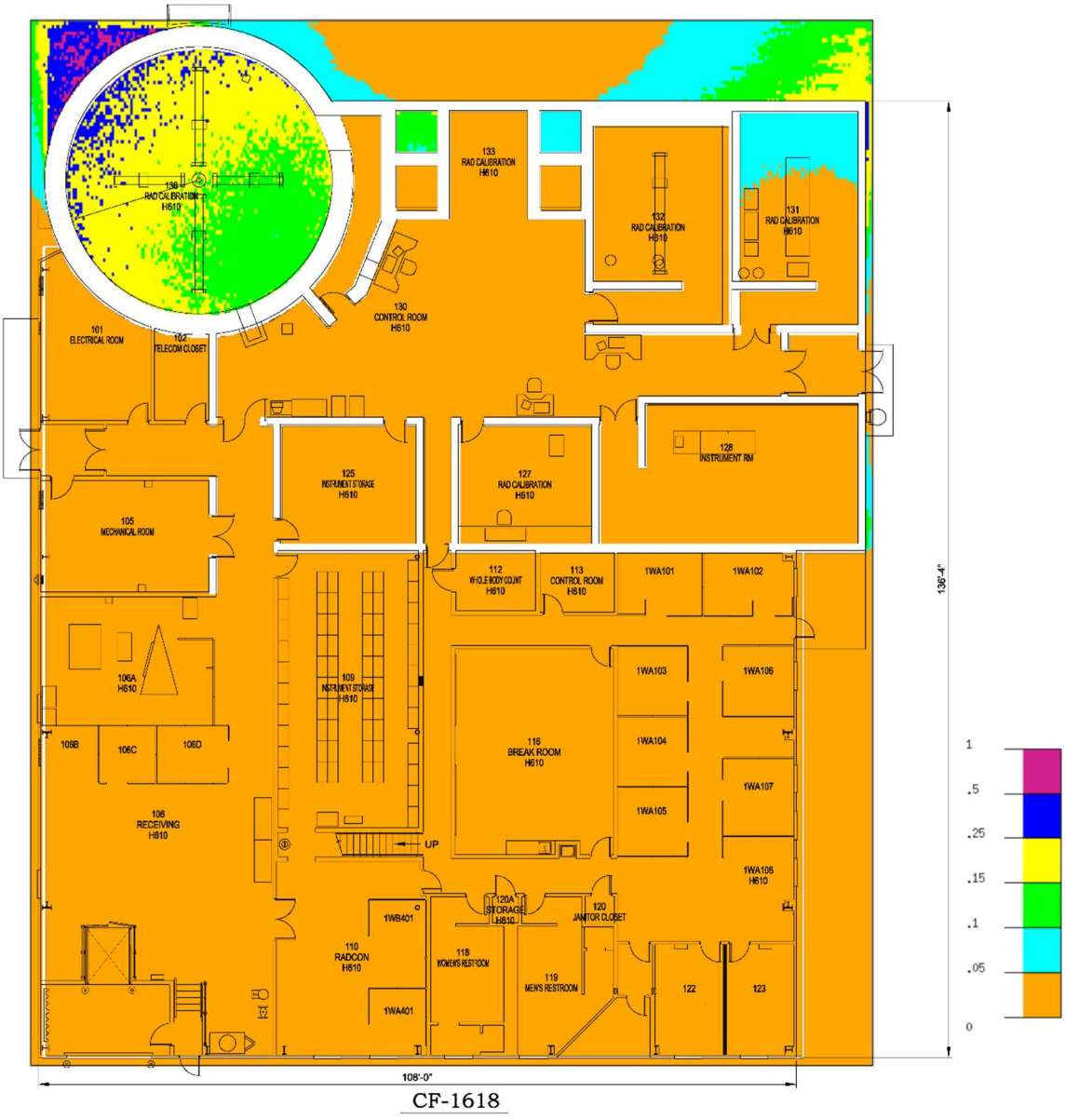

Figure 34: Source Position 4 Dose Rate Mesh Error Plot

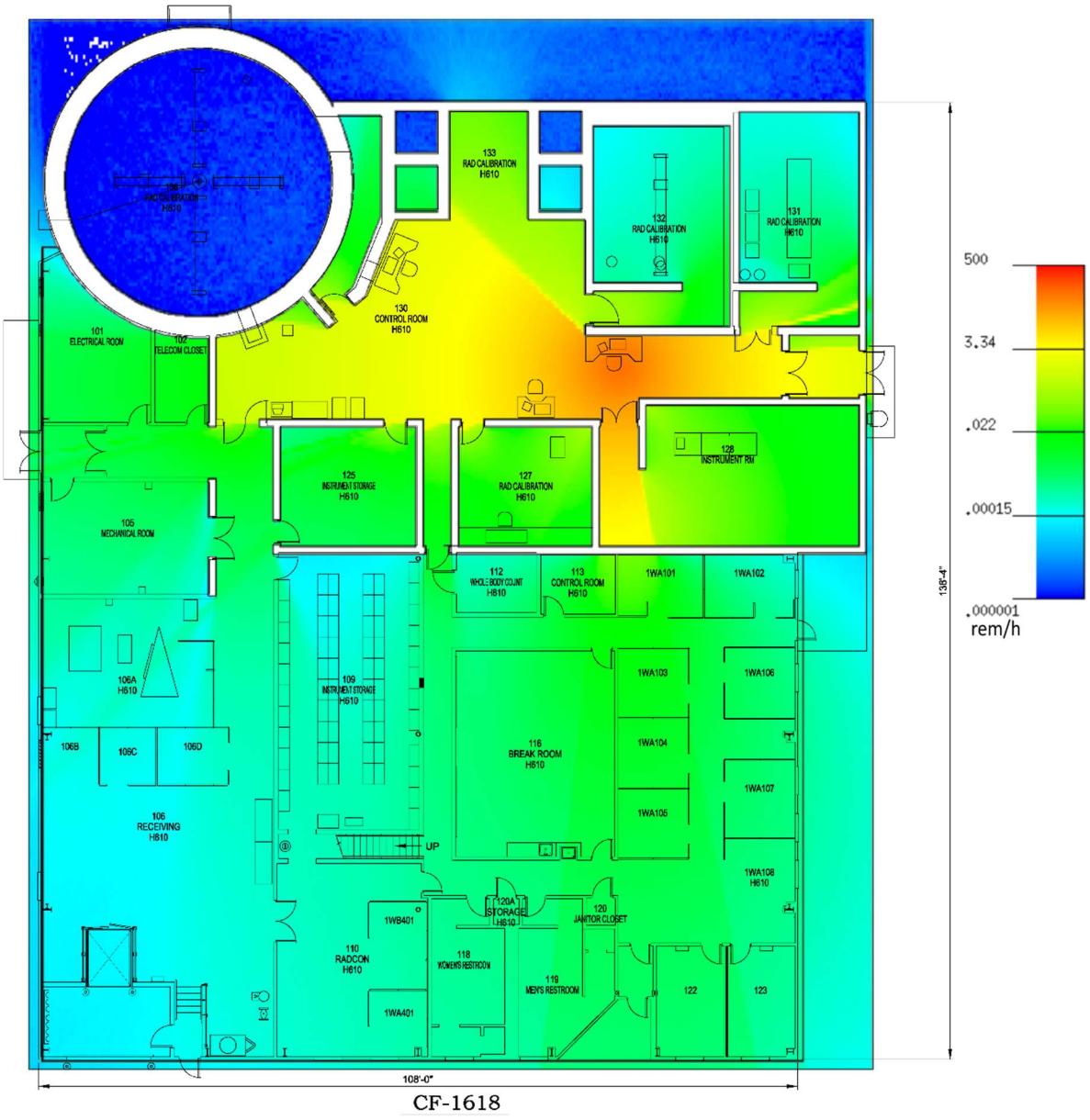

Figure 35: Source Position 5 Dose Rate (rem/h) Mesh

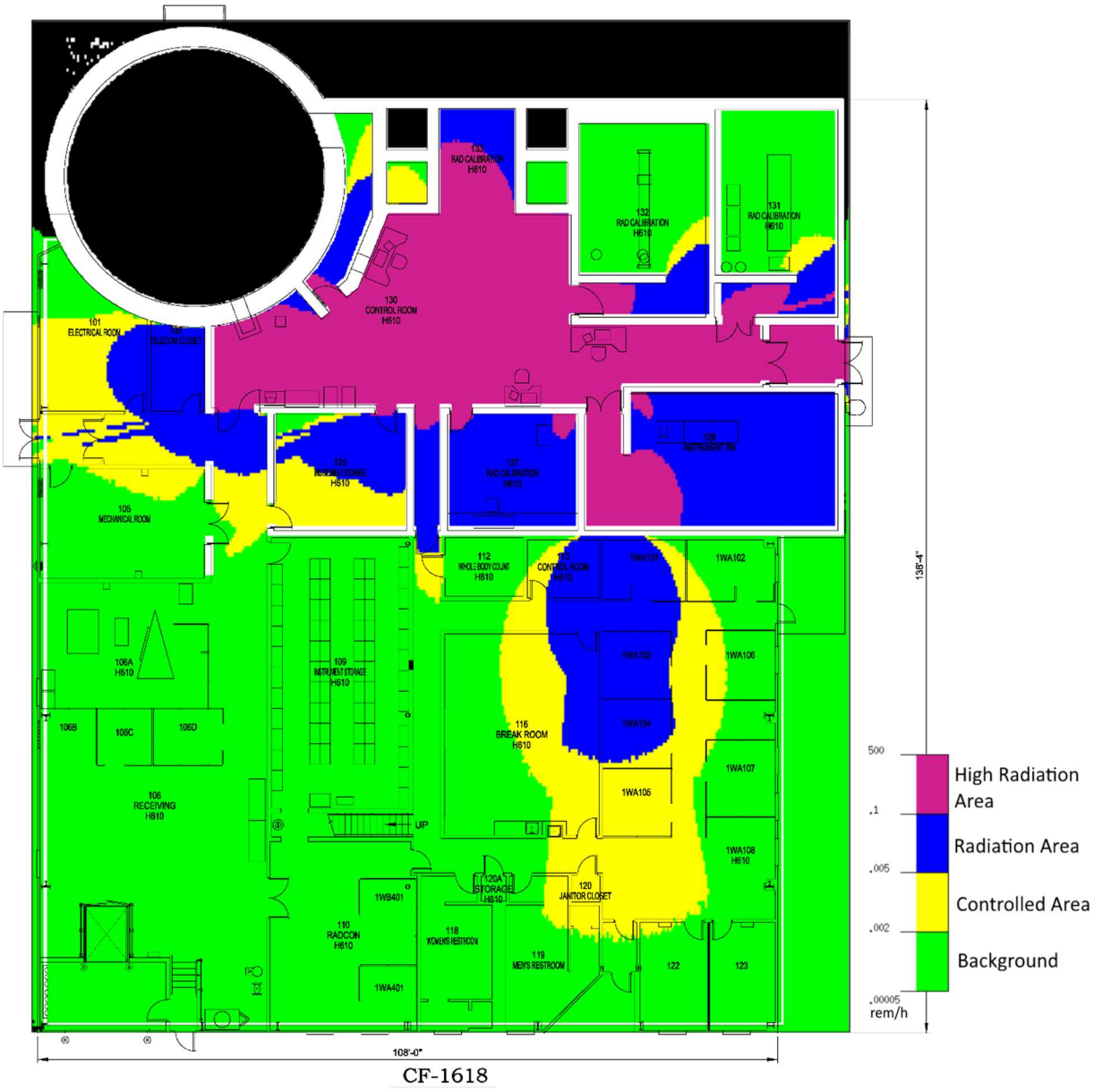

Figure 36: Radiation posting zones Source Position 5

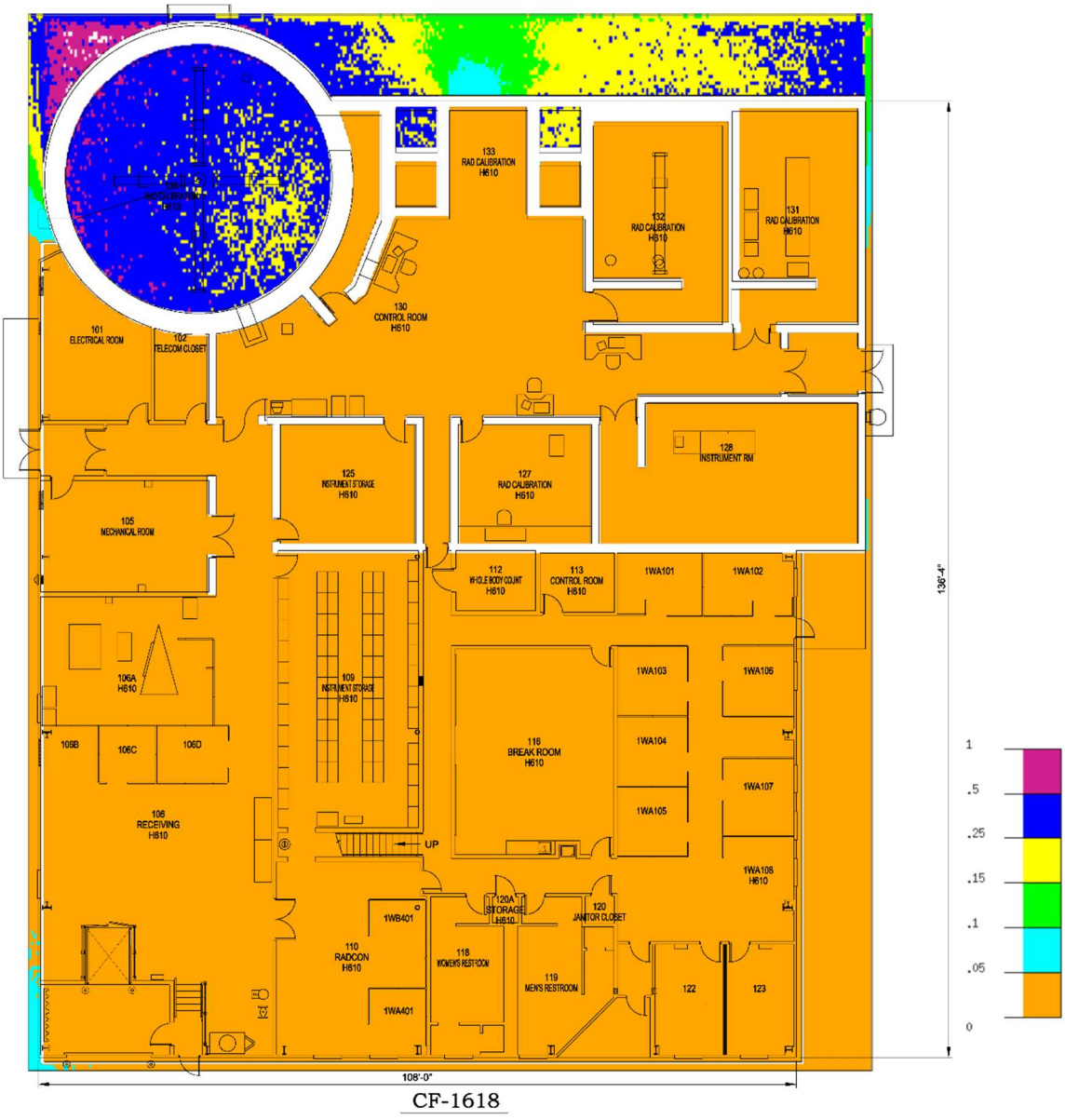

Figure 37: Source Position 5 Dose Rate Mesh Error Plot

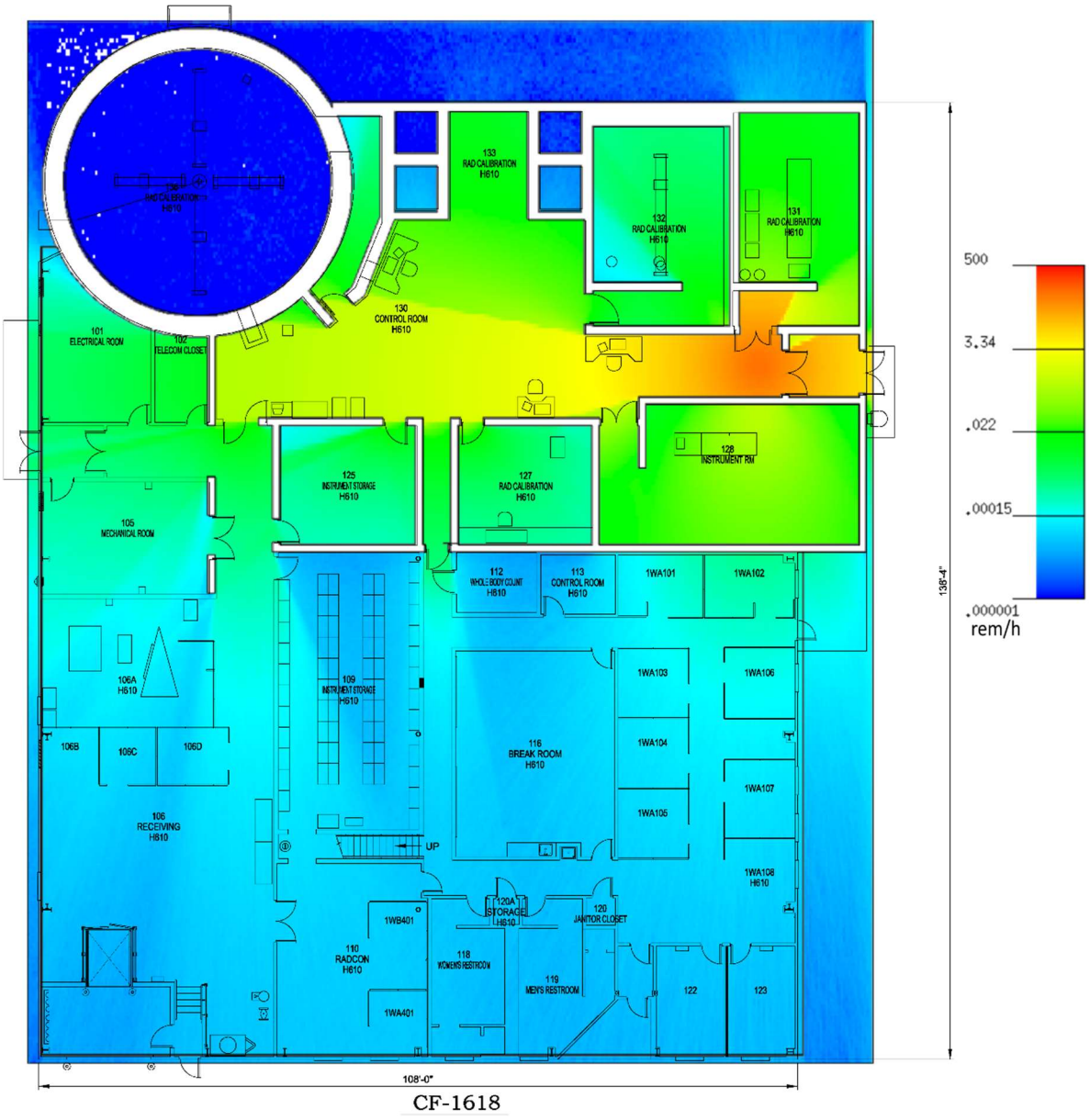

Figure 38: Source Position 6 Dose Rate (rem/h) Mesh

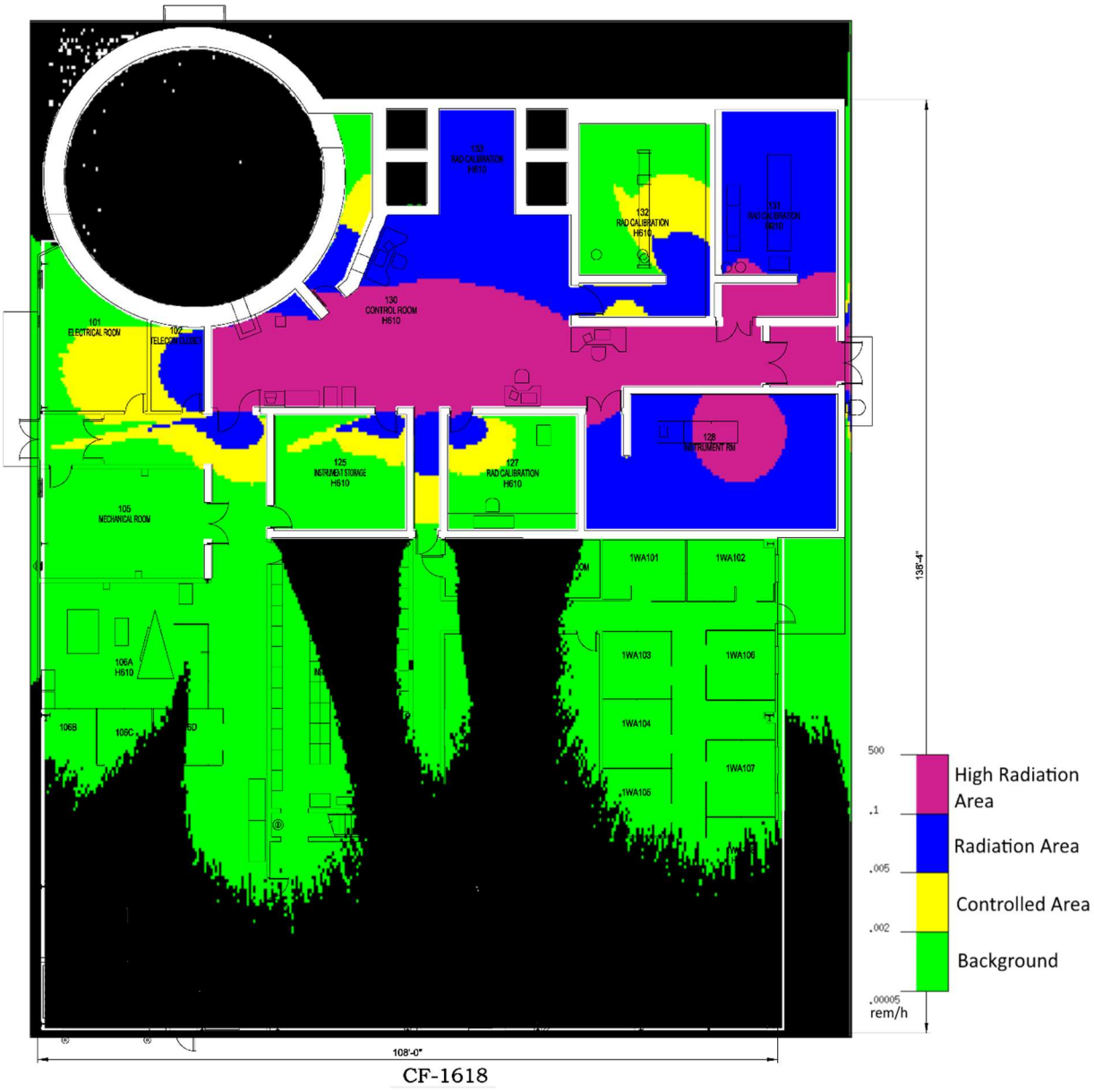

Figure 39: Radiation posting zones Source Position 6

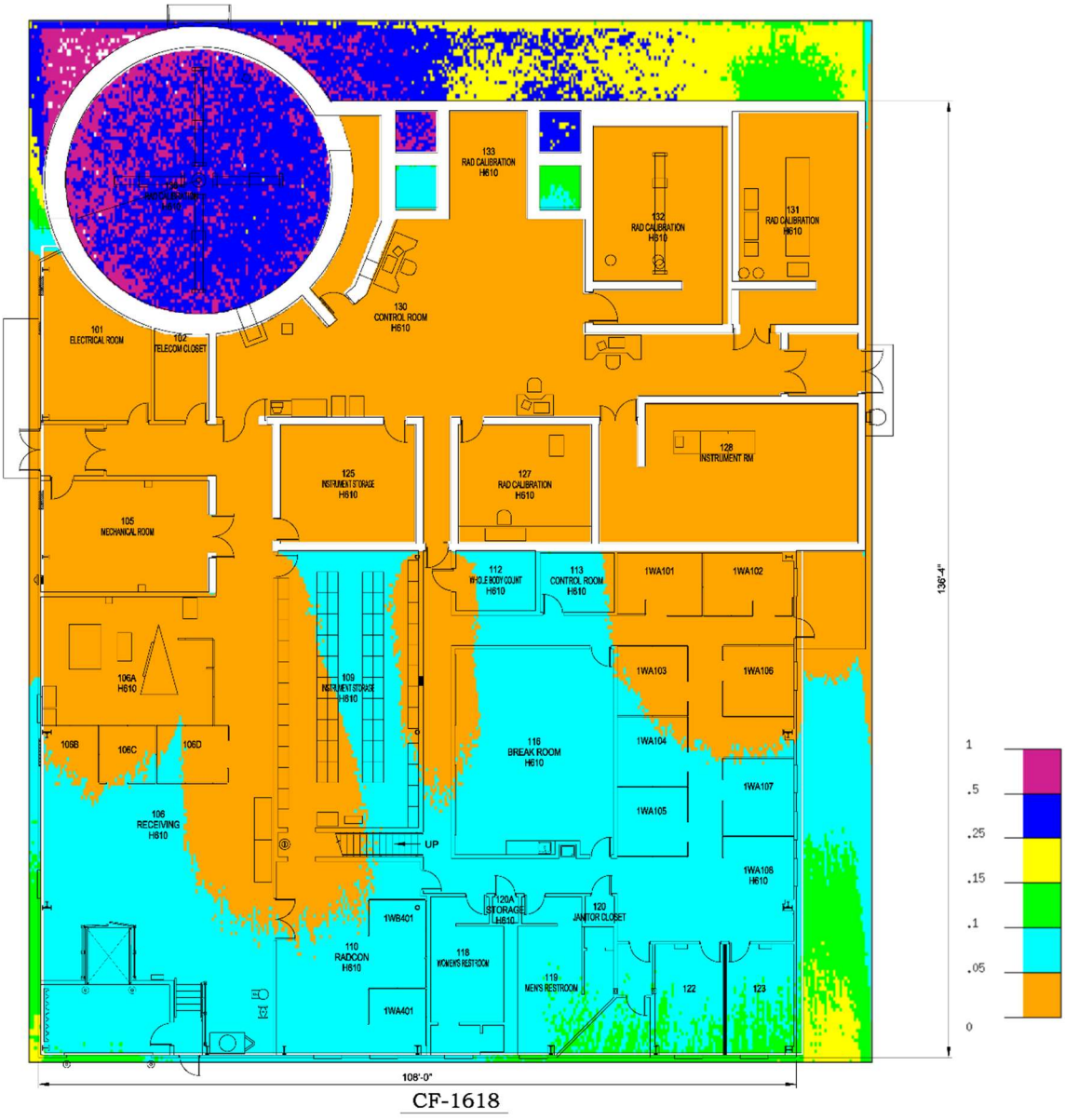

Figure 40: Source Position 6 Dose Rate Mesh Error Plot

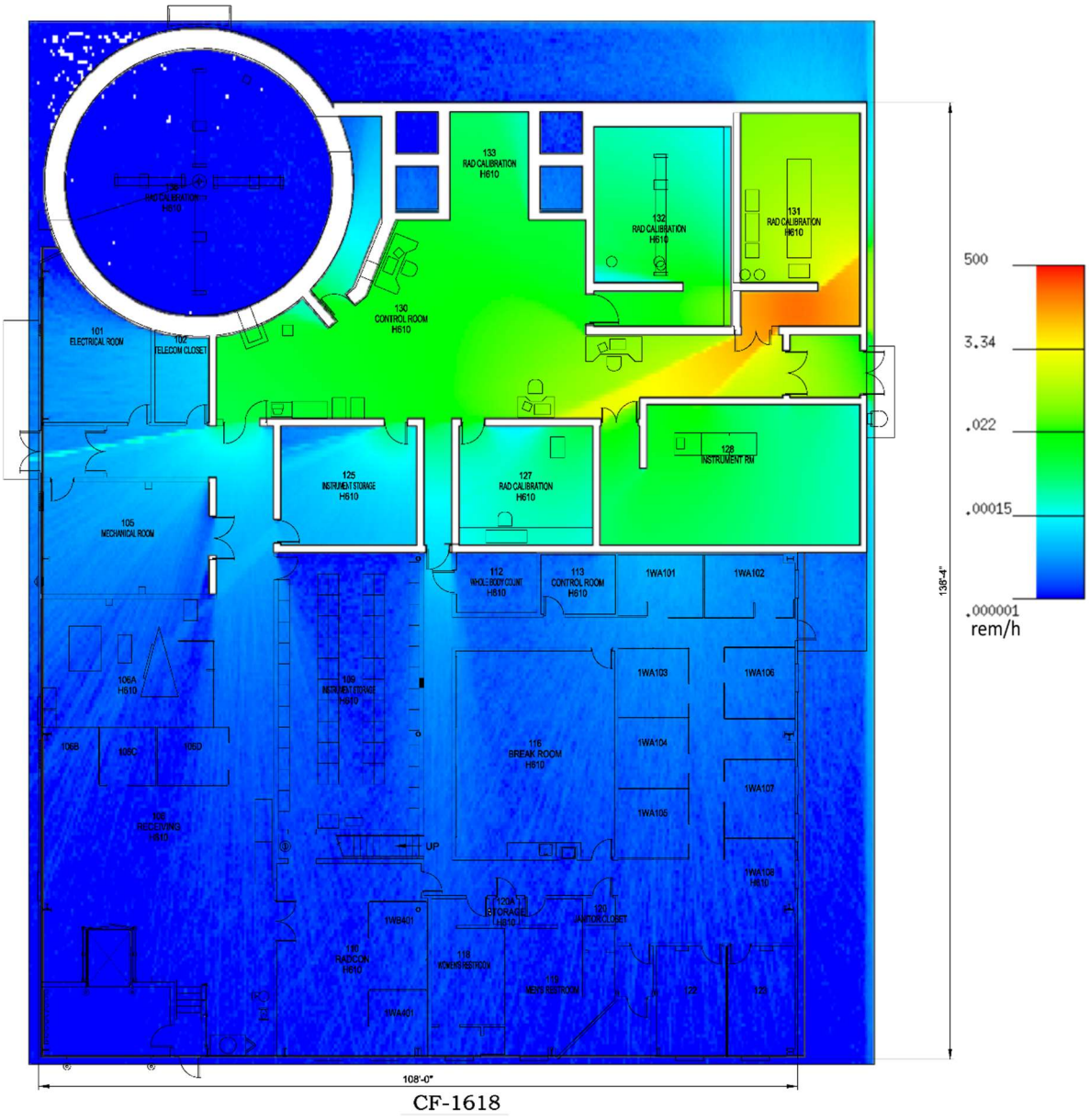

Figure 41: Source Position 7 Dose Rate (rem/h) Mesh

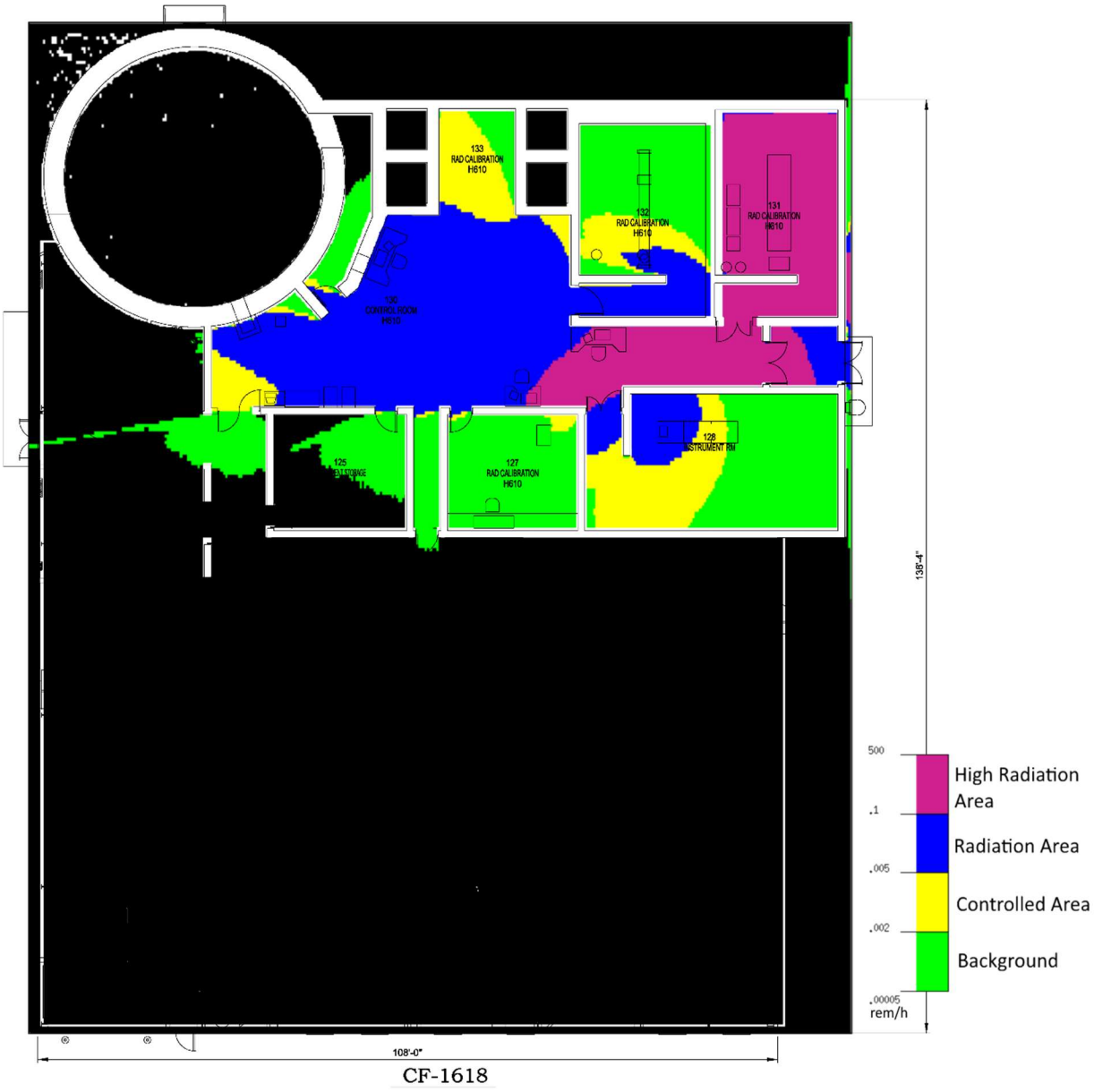

Figure 42: Radiation posting zones Source Position 7

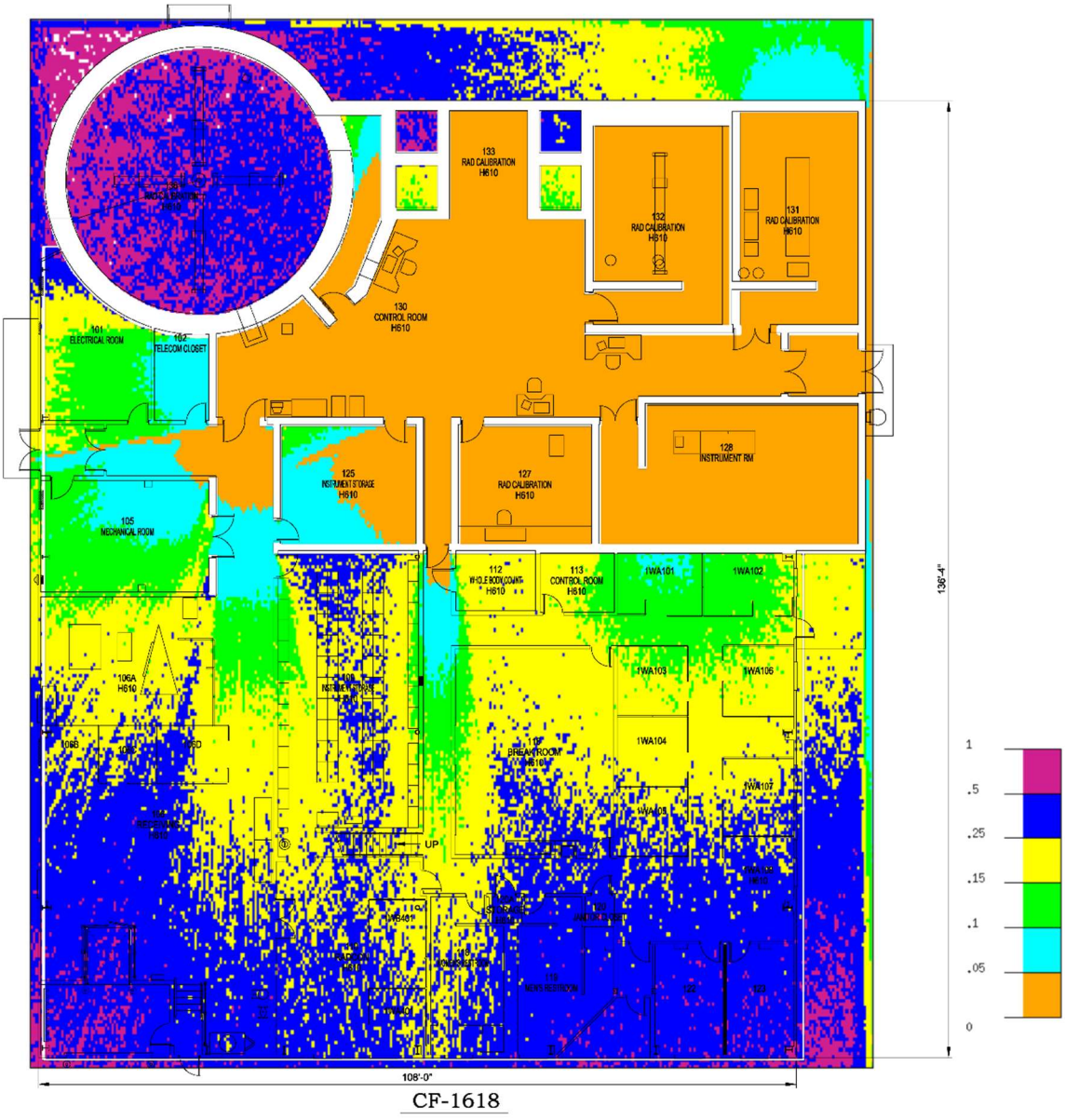

Figure 43: Source Position 7 Dose Rate Mesh Error Plot

Appendix B –MCNP Input Decks

```
MThompson HPIL Cs-137 Source Viewing Experimental Comparison Test Case Model
c Cell cards for HPIL Lab Geometry
  100   110   -2.25 -7 :(-8 9 ):-10 :-11 :-12 :(-13 14 ):-15 :-16 :
           (-17 18 ):-19 :-20 :-21 :-22 :-23 :-24 :-25 :-26 :-27 :
           (-29 30 ):-31 :-32 :-33 :(-34 35 36 ):(-37 38 ):-39 :-40 :
           (-41 42 43 44 45 46 ):-47 :-48 :-49 :(-50 51 ):
           (-52 53 ):-58 :-59  imp:p=1
  200   111   -2.32 -54 :(-55 29 ):-56 :(-57 52 )#100  imp:p=1
  300     0         -2 :4 :-1 :5 :-3 :6  imp:p=0   $outside universe
  400     4 -0.001205 2 -4 1 -5 3 -6 80 81 82 83 84 85 86 $all other equals air
           87 88 89 #100 #200 #300  imp:p=1
c Detectors
  500     4 -0.001205 -80  imp:p=1
  501     4 -0.001205 -81  imp:p=1
  502     4 -0.001205 -82  imp:p=1
  503     4 -0.001205 -83  imp:p=1
  504     4 -0.001205 -84  imp:p=1
  505     4 -0.001205 -85  imp:p=1
  506     4 -0.001205 -86  imp:p=1
  507     4 -0.001205 -87  imp:p=1
  508     4 -0.001205 -88  imp:p=1
  509     4 -0.001205 -89  imp:p=1

c All interior and exterior HPIL walls (North is neg y direction)
    1        py -350  $ North un
    2        px -30  $ East uni
    3        pz -460  $ Ground u
    4        px 3630  $ West uni
    5        py 4180  $ South un
    6        pz 560  $ Upper un
    7       rpp 0 3566.16 -320.04 4156 -15.25 0  $ Concrete
    8       rpp 0 30.48 0 1950.72 0 529  $ XBI/Inst
    9       rpp 0 30.48 1073 1263 0 213.36  $ East Lab
   10       rpp 30.48 548.64 0 45.72 0 529  $ XBI Prim
   11       rpp 548.64 589.28 0 970.28 0 529  $ XBI/GBI
   12       rpp 213.56 579.12 782.32 817.88 0 529  $ XBI inte
   13       rpp 30.48 1219.2 970.28 1005.84 0 529  $ XBI/GBI
   14       rpp 383.54 546.1 970.28 1005.84 0 213.36  $ XBI door
   15       rpp 589.28 1183.64 0 106.68 0 529  $ GBI Prim
   16       rpp 1183.64 1234.44 0 508 0 529  $ GBI/GWI
   17       rpp 1183.64 1219.2 508 1005.84 0 529  $ GBI cont
   18       rpp 1183.64 1219.2 833.12 965.2 0 213.36  $ GBI door
   19       rpp 797.56 1183.64 782.32 817.88 0 529  $ GBI labr
   20       rpp 1234.44 2042.16 0 40.64 0 529  $ GWI/GWL
   21       rpp 1234.44 1417.32 223.52 274.32 0 529  $ GWI 3/4
   22       rpp 1234.44 1417.32 475.2 508 0 529  $ GWI 4 la
   23       rpp 1417.32 1468.12 40.64 508 0 529  $ GWI 3/4
   24       rpp 1808.48 1859.28 40.64 508 0 529  $ GWI 1/2
   25       rpp 1859.28 2042.16 223.52 274.32 0 529  $ GWI 1/2
   26       rpp 1859.28 2042.16 475.2 508 0 529  $ GWI 1 la
   27       rpp 2042.16 2103.12 0 508 0 529  $ GWI/LSI
   c 28       rpp 2103.12 2321.56 0 50.8 0 529  $ LSI shor
   29       rcc 2895.6 350.52 0 0 0 529 670.56  $ LSI exte
   30       rcc 2895.6 350.52 0 0 0 529 579.12  $ LSI inte
   31       box 2042.16 508 0 131.62 331.3 0 56.65 -22.51 0 0 0 529  $ LSI labr
c 32  BOX 2173.78 839.3 0 161.87 139 0 39.71 -46.25 0 0 0 529         $ LSI labr
c 33  BOX 220.03 885.55 0 80.94 62.96 0 39.71 -46.25 0 0 0 213.36     $ LSI door
   32       box 2173.78 839.3 0 46.25 39.71 0 39.71 -46.25 0 0 0 529  $ LSI labr
   33       box 2300.97 948.51 0 34.689 29.784 0 114.2 -133 0 0 0 $ LSI labr
                529
   34       rpp 2821.305 2851.785 1005.84 2133.9175 0 529  $ Sentinal
   35       rpp 2821.305 2851.785 1402.08 1625.6 0 213.36  $ West exi
   36       rpp 2821.305 2851.785 1793.24 1966.2775 0 213.36  $ West mec
   37       rpp 335.28 365.76 1005.84 1280.16 0 529  $ XBI exit
   38       rpp 335.28 365.76 1076.96 1270 0 213.36  $ XBI exit
   39       rpp 30.48 985.52 1280.16 1310.64 0 529  $ Instrume
   40       rpp 955.04 985.52 1310.64 1584.96 0 529  $ Instrume
   41       rpp 985.52 2851.785 1371.6 1402.08 0 529  $ Count ro
```

```
   42       rpp 990.6 1153.16 1371.6 1402.08 0 213.36  $ Instrume
   43       rpp 1656.08 1757.68 1371.6 1402.08 0 213.36  $ Count ro
   44       rpp 1798.32 1920.24 1317.6 1402.08 0 529  $ Lab exit
   45       rpp 1991.36 2092.96 1317.6 1402.08 0 213.36  $ Storage
   46       rpp 2629.8525 2822.8925 1317.6 1402.08 0 213.36  $ Sentinal
   47       rpp 1158.24 1188.72 1402.08 1920.24 0 529  $ Instrume
   48       rpp 1767.84 1798.32 1402.08 1920.24 0 529  $ Count ro
   49       rpp 1920.24 1950.72 1402.08 1920.24 0 529  $ Storage
   50       rpp 2540 2570.48 1402.08 1920.24 0 529  $ Storage
   51       rpp 2540 2570.48 1808.48 1910.08 0 213.36  $ Storage
   52       rpp 30.48 2570.48 1920.24 1950.72 0 529  $ Wall bet
   53       rpp 1808.48 1910.08 1920.24 1950.72 0 213.36  $ Lab hall
   54       rpp 3571.24 3572.8275 629.92 4142.75 0 529  $ West ext
   55       rpp 3479.8 3571.24 629.92 631.5075 0 529  $ West LSI
   56       rpp 271.9875 3571.24 4141.1525 4142.74 0 529  $ South ex
   57       rpp 270.4 271.9875 1950.72 4142.74 0 529  $ East ext
   58       rpp 0 3566.16 -320.04 4156 529 544.24  $ 6 inch c
   59       rpp 2042.16 2310.6 0 60.96 0 529  $LSI Labrynth exterior wall
c
c Detector Definitions
c
   80         s 891.54 112.68 162.56 5  $GBI far wall pos 1 RDS31
   81         s 889 823.88 156.21 5  $GBI Labryinth Wall pos 2 RDS31
   82         s 1036.32 1011.84 121.94 5  $GBI Hall Wall pos 3 RDS31
   83         s 36.48 1050.14 121.94 5  $XBI Exit Area pos 4 DMC3000
   84         s 802.64 1316.64 121.92 5  $Instrument Shop pos 5 DMC3000
   85         s 925.72 1956.72 121.92 5  $Kevin's Office pos 6 RDS31
   86         s 1630.68 1408.08 121.92 5  $Count Room pos 7 DMC3000
   87         s 1914.24 1889.76 121.92 5  $Lab Hallway Ent pos 8 DMC3000
   88         s 2815.305 1287.12 121.92 5  $Sentinal Comp Exit pos 9 DMC3000
   89         s 1300.48 754.38 139.7 5  $GBI Control Cabinet pos 10 RDS31

mode  p
c J.E. Tanner's Best Concrete  2.25 g/cc  7.359E-02 at/b-cm  JET-03-91
m110  6000.            0.0016
      8016.          0.043394 8017.        1.653e-005 11023.          0.00055
      13027.           0.0016 14028.         0.014018 14029.       0.00071212
      14030.       0.00046998 16032.      4.7495e-005 16033.        3.75e-007
      16034.       2.125e-006 16036.           5e-009 20040.        0.0030052
      20042.      2.0057e-005 20043.       4.185e-006 20044.      6.4666e-005
      20046.        1.24e-007 20048.       5.797e-006 26054.      2.2211e-005
      26056.       0.00034867 26057.      8.0522e-006 26058.      1.0716e-006
      1001.         0.0076051 1002.       8.7469e-007
c
c Air (dry, near sea level)  0.001205 g/cc  5.0000E-05 at/b-cm  PNNL-15870 Rev2
c The above density is estimated to be accurate to 4 significant digits. Uncerta
c Dry air near sea level
c The NIST data yields a CO2 content in air of about 299 ppm by volume whereas m
m4    6000.          0.000151
      7014.          0.781574 7015.          0.002855 8016.          0.210238
      8017.            8e-005 18036.         1.6e-005 18038.           3e-006
      18040.         0.004653
c
c Gypsum (Plaster of Paris) PNNL-15870 Rev 2 #162
c The density varies for diff types of gypsum, using 2.32 g/cm^3
m111  1000.         -0.023416
      8000.         -0.557572 16000.        -0.186215 20000.        -0.232797
c source definition Cs-137
sdef ERG=D1 POS= 871.22 690.88 143.1417 PAR=P
si1 L 0.662
sp1 D 1
c Tally Definition
f4:p 500 501 502 503 504 505 506 507 508 509
fm4 8.91e16 $Source Strength in photons/hr
c Values from ICRP116 converted from pSv cm^2 to rem cm^2 to produce rem/hr results
de log  0.01 0.015 0.02 0.03 0.04 0.05 0.06 0.07 0.08 0.1 0.15
        0.2 0.3 0.4 0.5 0.511 0.6 0.662 0.8 1
df log  2.88e-12 5.6e-12 8.12e-12 1.27e-11 1.58e-11 1.8e-11 1.99e-11
        2.18e-11 2.39e-11 2.87e-11 4.29e-11 5.89e-11 9.32e-11 1.28e-10
               1.63e-10 1.67e-10 1.97e-10 2.17e-10 2.62e-10 3.25e-10
nps 1E11
```

```
prdmp  1e10 1e10 0 1
print
```

Figure 44: Detector Experimental Comparison Test Case MCNP Input Deck

```
MThompson HPIL Cs-137 Source Viewing Mesh Model
c Cell cards for HPIL Lab Geometry
  100   110   -2.25 -7 :(-8 9 ):-10 :-11 :-12 :(-13 14 ):-15 :-16 :
            (-17 18 ):-19 :-20 :-21 :-22 :-23 :-24 :-25 :-26 :-27 :
            (-29 30 ):-31 :-32 :-33 :(-34 35 36 ):(-37 38 ):-39 :-40 :
            (-41 42 43 44 45 46 ):-47 :-48 :-49 :(-50 51 ):
            (-52 53 ):-58 :-59  imp:p=1
  200   111   -2.32 -54 :(-55 29 ):-56 :(-57 52 )#100  imp:p=1
  300     0         -2 :4 :-1 :5 :-3 :6  imp:p=0   $outside universe
  400     4 -0.001205 2 -4 1 -5 3 -6 $all other equals air
              #100 #200 #300  imp:p=1

c All interior and exterior HPIL walls (North is neg y direction)
    1        py -350  $ North un
    2        px -30  $ East uni
    3        pz -460  $ Ground u
    4        px 3630  $ West uni
    5        py 4180  $ South un
    6        pz 560  $ Upper un
    7       rpp 0 3566.16 -320.04 4156 -15.25 0  $ Concrete
    8       rpp 0 30.48 0 1950.72 0 529  $ XBI/Inst
    9       rpp 0 30.48 1073 1263 0 213.36  $ East Lab
   10       rpp 30.48 548.64 0 45.72 0 529  $ XBI Prim
   11       rpp 548.64 589.28 0 970.28 0 529  $ XBI/GBI
   12       rpp 213.56 579.12 782.32 817.88 0 529  $ XBI inte
   13       rpp 30.48 1219.2 970.28 1005.84 0 529  $ XBI/GBI
   14       rpp 383.54 546.1 970.28 1005.84 0 213.36  $ XBI door
   15       rpp 589.28 1183.64 0 106.68 0 529  $ GBI Prim
   16       rpp 1183.64 1234.44 0 508 0 529  $ GBI/GWI
   17       rpp 1183.64 1219.2 508 1005.84 0 529  $ GBI cont
   18       rpp 1183.64 1219.2 833.12 965.2 0 213.36  $ GBI door
   19       rpp 797.56 1183.64 782.32 817.88 0 529  $ GBI labr
   20       rpp 1234.44 2042.16 0 40.64 0 529  $ GWI/GWL
   21       rpp 1234.44 1417.32 223.52 274.32 0 529  $ GWI 3/4
   22       rpp 1234.44 1417.32 475.2 508 0 529  $ GWI 4 la
   23       rpp 1417.32 1468.12 40.64 508 0 529  $ GWI 3/4
   24       rpp 1808.48 1859.28 40.64 508 0 529  $ GWI 1/2
   25       rpp 1859.28 2042.16 223.52 274.32 0 529  $ GWI 1/2
   26       rpp 1859.28 2042.16 475.2 508 0 529  $ GWI 1 la
   27       rpp 2042.16 2103.12 0 508 0 529  $ GWI/LSI
   29       rcc 2895.6 350.52 0 0 0 529 670.56  $ LSI exte
   30       rcc 2895.6 350.52 0 0 0 529 579.12  $ LSI inte
   31       box 2042.16 508 0 131.62 331.3 0 56.65 -22.51 0 0 0 529  $ LSI labr
   32       box 2173.78 839.3 0 46.25 39.71 0 39.71 -46.25 0 0 0 529  $ LSI labr
   33       box 2300.97 948.51 0 34.689 29.784 0 114.2 -133 0 0 0 $ LSI labr
                529
   34       rpp 2821.305 2851.785 1005.84 2133.9175 0 529  $ Sentinal
   35       rpp 2821.305 2851.785 1402.08 1625.6 0 213.36  $ West exi
   36       rpp 2821.305 2851.785 1793.24 1966.2775 0 213.36  $ West mec
   37       rpp 335.28 365.76 1005.84 1280.16 0 529  $ XBI exit
   38       rpp 335.28 365.76 1076.96 1270 0 213.36  $ XBI exit
   39       rpp 30.48 985.52 1280.16 1310.64 0 529  $ Instrume
   40       rpp 955.04 985.52 1310.64 1584.96 0 529  $ Instrume
   41       rpp 985.52 2851.785 1371.6 1402.08 0 529  $ Count ro
   42       rpp 990.6 1153.16 1371.6 1402.08 0 213.36  $ Instrume
   43       rpp 1656.08 1757.68 1371.6 1402.08 0 213.36  $ Count ro
   44       rpp 1798.32 1920.24 1317.6 1402.08 0 529  $ Lab exit
   45       rpp 1991.36 2092.96 1317.6 1402.08 0 213.36  $ Storage
   46       rpp 2629.8525 2822.8925 1317.6 1402.08 0 213.36  $ Sentinal
   47       rpp 1158.24 1188.72 1402.08 1920.24 0 529  $ Instrume
   48       rpp 1767.84 1798.32 1402.08 1920.24 0 529  $ Count ro
   49       rpp 1920.24 1950.72 1402.08 1920.24 0 529  $ Storage
   50       rpp 2540 2570.48 1402.08 1920.24 0 529  $ Storage
   51       rpp 2540 2570.48 1808.48 1910.08 0 213.36  $ Storage
   52       rpp 30.48 2570.48 1920.24 1950.72 0 529  $ Wall bet
   53       rpp 1808.48 1910.08 1920.24 1950.72 0 213.36  $ Lab hall
   54       rpp 3571.24 3572.8275 629.92 4142.75 0 529  $ West ext
   55       rpp 3479.8 3571.24 629.92 631.5075 0 529  $ West LSI
   56       rpp 271.9875 3571.24 4141.1525 4142.74 0 529  $ South ex
```

```
   57       rpp 270.4 271.9875 1950.72 4142.74 0 529  $ East ext
   58       rpp 0 3566.16 -320.04 4156 529 544.24  $ 6 inch c
   59       rpp 2042.16 2310.6 0 60.96 0 529  $LSI Labrynth exterior wall

mode  p
c J.E. Tanner's Best Concrete  2.25 g/cc  7.359E-02 at/b-cm  JET-03-91
m110  6000.            0.0016
      8016.          0.043394 8017.        1.653e-005 11023.          0.00055
      13027.           0.0016 14028.         0.014018 14029.       0.00071212
      14030.       0.00046998 16032.      4.7495e-005 16033.        3.75e-007
      16034.       2.125e-006 16036.           5e-009 20040.        0.0030052
      20042.      2.0057e-005 20043.       4.185e-006 20044.      6.4666e-005
      20046.        1.24e-007 20048.       5.797e-006 26054.      2.2211e-005
      26056.       0.00034867 26057.      8.0522e-006 26058.      1.0716e-006
      1001.         0.0076051 1002.       8.7469e-007
c
c Air (dry, near sea level)  0.001205 g/cc  5.0000E-05 at/b-cm  PNNL-15870 Rev2
c The above density is estimated to be accurate to 4 significant digits. Uncerta
c Dry air near sea level
c The NIST data yields a CO2 content in air of about 299 ppm by volume whereas m
m4    6000.          0.000151
      7014.          0.781574 7015.          0.002855 8016.          0.210238
      8017.            8e-005 18036.         1.6e-005 18038.           3e-006
      18040.         0.004653
c
c Gypsum (Plaster of Paris) PNNL-15870 Rev 2 #162
c The density varies for diff types of gypsum, using 2.32 g/cm^3
m111  1000.         -0.023416
      8000.         -0.557572 16000.        -0.186215 20000.        -0.232797
c source definition Cs-137
sdef ERG=D1 POS= 871.22 690.88 143.1417 PAR=P
si1 L 0.662
sp1 D 1
c Mesh Tally Definition
FMESH4:p GEOM=xyz ORIGIN=-30 -350 120
        IMESH=3630 IINTS=366
        JMESH=4180 JINTS=453
        KMESH=165 KINTS=1
        OUT=ij
fm4 8.91e16 $Source Strength in photons/hr
c Values from ICRP116 converted from pSv cm^2 to rem cm^2 to produce rem/hr results
de log  0.01 0.015 0.02 0.03 0.04 0.05 0.06 0.07 0.08 0.1 0.15
        0.2 0.3 0.4 0.5 0.511 0.6 0.662 0.8 1
df log  2.88e-12 5.6e-12 8.12e-12 1.27e-11 1.58e-11 1.8e-11 1.99e-11
        2.18e-11 2.39e-11 2.87e-11 4.29e-11 5.89e-11 9.32e-11 1.28e-10
              1.63e-10 1.67e-10 1.97e-10 2.17e-10 2.62e-10 3.25e-10
nps 1E11
prdmp  1e10 1e10 0 1
print
```

Figure 45: Source Viewing Mesh MCNP Input Deck